DOI: 10.1111/cmi.13392

RESEARCH ARTICLE



Check for updates

Blockade of endoplasmic reticulum stress-induced cell death by *Ureaplasma parvum* vacuolating factor

Fumiko Nishiumi¹ | Yasuhiro Kawai^{1,2} | Yukiko Nakura¹ | Michinobu Yoshimura^{1,3} | Heng Ning Wu¹ | Mitsuhide Hamaguchi^{4,5} | Shigeyuki Kakizawa⁶ | Yo Suzuki⁷ | John I. Glass⁷ | Itaru Yanagihara¹ |

Correspondence

Itaru Yanagihara, Department of Developmental Medicine, Research Institute, Osaka Women's and Children's Hospital, 840 Murodo-cho, Izumi-City, Osaka 594-1101, Japan.

Email: itaruy@mch.pref.osaka.jp

Funding information

Biomedical Engineering Research from Nakatani Foundation, Grant/Award Number: 2018T006; Japan Agency for Medical Research and Development, Grant/Award Number: JP20fk0108143; Japan Society for the Promotion of Science, Grant/Award Numbers: JP17H04237, JP17K10201, JP18K16788, JP18K19191, JP19K07569, JP20H03564, JP26860859; United States National Science Foundation MCB program, Grant/Award Numbers: 1818344, 1840320

Abstract

Previously, we found that Ureaplasma parvum internalised into HeLa cells and cytosolic accumulation of galectin-3. U. parvum induced the host cellular membrane damage and survived there. Here, we conducted vesicular trafficking inhibitory screening in yeast to identify U. parvum vacuolating factor (UpVF). U. parvum triggered endoplasmic reticulum (ER) stress and upregulated the unfolded protein response-related factors, including BiP, P-eIF2 and IRE1 in the host cells, but it blocked the induction of the downstream apoptotic factors. MicroRNA library screening of U. parvuminfected cells and UpVF-transfected cells identified miR-211 and miR-214 as the negative regulators of the apoptotic cascade under ER stress. Transient expression of UpVF induced HeLa cell death with intracellular vacuolization; however, some stable UpVF transformant survived. U. parvum-infected cervical cell lines showed resistance to actinomycin D, and UpVF stable transformant cell lines exhibited resistance to Xray irradiation, as well as cisplatin and paclitaxel. UpVF expressing cervical cancer xenografts in nude mice also acquired resistance to cisplatin and paclitaxel. A mycoplasma expression vector based on Mycoplasma mycoides, Syn-MBA (multiple banded antigen)-UpVF, reduced HeLa cell survival compared with that of Syn-MBA after 72 hr of infection. These findings together suggest novel mechanisms for Ureaplasma infection and the possible implications for cervical cancer malignancy.

Take Aways

- Ureaplasmal novel virulence factor, UpVF, was identified.
- UpVF triggered ER stress but suppressed apoptotic cascade via miR-211 and -214.
- UpVF conferred resistance to anticancer treatments both in vivo and in vitro.
- Dual expression of MBA and UpVF in JCVI-syn3B showed host cell damage.

KEYWORDS

cervical cancer, ER stress, miRNA, Ureaplasma parvum, vacuolating factor

¹Department of Developmental Medicine, Research Institute, Women's and Children's Hospital, Osaka, Japan

²Health Evaluation Center, Kanazawa Medical University Himi Municipal Hospital, Toyama, Japan

³Department of Microbiology and Immunology, Faculty of Medicine, Fukuoka University, Fukuoka, Japan

⁴Department of Anesthesia, Critical Care and Pain Medicine, Massachusetts General Hospital, Harvard Medical School, Boston, Massachusetts, USA

⁵Department of Emergency and Critical Care Medicine, Kindai University Faculty of Medicine, Osaka, Japan

⁶Bioproduction Research Institute,, National Institute of Advanced Industrial Science and Technology, Tsukuba, Japan

⁷Synthetic Biology Group, J. Craig Venter Institute, La Jolla, California, USA

1 | INTRODUCTION

Chronic inflammation predisposes patients to cancer (Maman & Witz, 2018). Approximately 20% of all human cancer cases worldwide are known to be caused by infectious microbes, including Epstein-Barr virus, hepatitis C virus, human papillomavirus (HPV) and Helicobacter pylori (Mager, 2006; White, Pagano, & Khalili, 2014). Mycoplasmas, which are associated with persistent infection, are atypical bacteria that evolved from conventional bacteria through massive gene loss enabled by their obligate parasitic lifestyle. Their salient characteristic is a lack of a cell wall. Because mycoplasmas have extremely small genomes (0.58-2.20 Mb), these organisms have limited metabolic options for survival and depend on the host or growth medium to supply exogenous nutrients, including sterols (Kornspan & Rottem, 2012). Numerous studies have reported associations between some mycoplasmas and cancer dating back to the 1960s (Ning & Shou, 2004; Ye et al., 2018; Zarei, Rezania, & Mousavi, 2013). Example of mycoplasma-cancer linkage includes: Mycoplasma hyorhinis and gastric cancer, Mycoplasma hominis and Mycoplasma genitalium (Miyake et al., 2019; Namiki et al., 2009) and prostate cancer (Rogers, 2011), and Ureaplasma urealyticum and cervical cancer (Xiaolei, Taot, Zongli, & Hongying, 2014). Furthermore, U. urealyticum has been reported to be a possible enhancer of HPVinduced cervical cancer (Drago et al., 2016). Recently, Zella et al., (Zella et al., 2018) showed that Mycoplasma fermentans DnaK is responsible for lymphomagenesis in SCID mice. Tumour-associated mycoplasmas may decrease the therapeutic efficiency of gemcitabine via mycoplasma-encoded cytidine deaminase nucleoside phosphorylase (Vande Voorde et al., 2014).

Galectin-3 binds to β -galactoside glycoconjugates and accumulates in host cells when it becomes exposed to the cytosol upon membrane damage within phagosomes harbouring bacteria with membrane-penetrating properties (Chauhan et al., 2016). There, it regulates antibacterial autophagy (Weng et al., 2018). Galectin-3 is also known to be a diverse regulator of cancer cell activities, including transformation, growth, metastasis and apoptosis (Newlaczyl & Yu, 2011). We previously reported that $U.\ parvum$ internalised into HeLa cells by clathrin-mediated endocytosis, resulting in the cytosolic accumulation of galectin-3 at the site of bacterial internalisation (Nishiumi et al., 2017). The internalised $U.\ parvum$ was subsequently entrapped by the autophagy marker LC3. Even though $U.\ parvum$ damaged the host cellular membrane and the process of autophagy was mobilised, the host cell and $U.\ parvum$ co-existed in a delicate balance between the host and the obligate microbe.

When protein folding requirements exceed the endoplasmic reticulum (ER) processing capacity, unfolded proteins accumulate, induce ER stress and trigger the unfolded protein response (UPR), which is an evolutionarily conserved cytoprotective signalling pathway (Ma & Hendershot, 2004). Inflammation induces ER stress and altered mitochondrial function resulting in reactive oxygen species (ROS) production (Delmotte & Sieck, 2019). ER stress and oxidative stress are highly interrelated biological processes that regulate a wide range of signalling pathways in the cell (Cao & Kaufman, 2014). Recent works focused on the molecular interactions between mitochondria and ER

contact sites, such as 54-amino acid microprotein PIGBOS (Chu et al., 2019). Cancer cells re-establish ER homeostasis through UPR, which aids cell survival, in response to various stresses, such as oxygen deprivation, nutrient deprivation and various cancer therapies (Chandrahas, Han, & Kaufman, 2018; Madden, Logue, Healy, Manie, & Samali, 2019; Papaioannou & Chevet, 2018). The UPR is initiated when unfolded proteins within the ER excessively bind the glucoseregulated chaperone BiP/GRP78, titrating it away from three primary stress sensors in the ER membrane: inositol-requiring enzyme 1 (IRE1), activating transcription factor 6 (ATF6) and PKR-like endoplasmic reticulum kinase (PERK). These three primary UPR signalling molecules are crucial for oncogenesis and tumour growth, metastasis and resistance to treatment (Avril, Vauleon, & Chevet, 2017; Urra, Dufey, Avril, Chevet, & Hetz, 2016). The discovery of a functional connection between UPR signalling and microRNAs (miRNAs) has revealed another layer of complexity in the regulation and progression of various cancers, including cervical cancer and cervical cancer cell lines (Pardini et al., 2018), Downstream of PERK, ATF4-dependent expression of miR-211 and NRF2-dependent expression of miR-214 promote cell survival. miR-211 contains a sequence targeting the promoter region of chop, and suppressed expression of chop inhibits proapoptotic signalling and aids cell survival. Decreased expression of miR-214 enables ATF4 expression, which increases the transcription of prosurvival genes (McQuiston & Diehl, 2017; Penna, Orso, & Taverna, 2015), miR-214 suppresses the growth and invasiveness of cervical cancer cells by targeting GALNT7 (Peng et al., 2012), miR-211 inhibits the proliferation, invasion, and migration of cervical cancer cells by targeting SPARC (Qu et al., 2018). Evidence shows that the specific target genes of each of these miRNAs affect cellular fate under various stresses that are now accumulating.

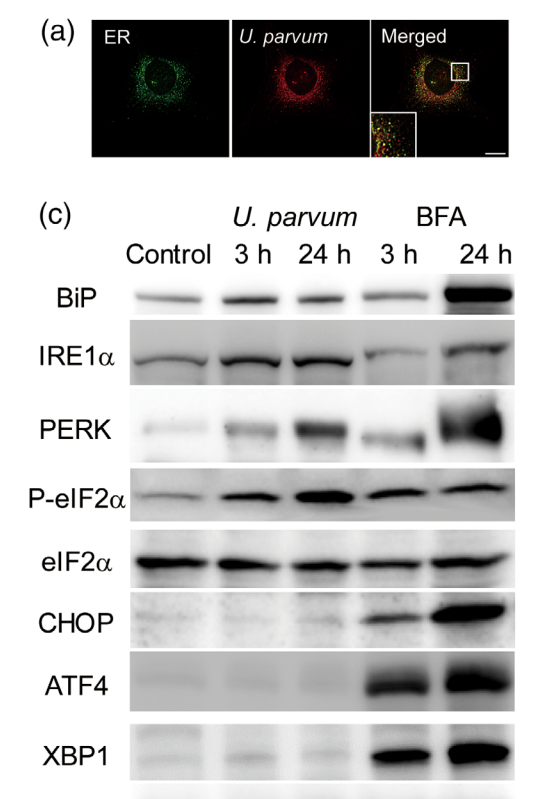
Ureaplasma spp. have a high incidence in vaginal swabs collected from healthy reproductive-age women (Tantengco & Yanagihara, 2019). It is not yet known how *U. parvum* achieves long-term colonisation despite various host cellular responses to stress. In the present report, we identify a novel virulence factor from *U. parvum*, *U. parvum* vacuolating factor (UpVF). In cervical cancer cell lines, UpVF showed anti-apoptotic properties under X-ray irradiation and treatment with anticancer drugs. Additionally, xenografted UpVF-expressing CaSki cells showed resistance to both cisplatin and paclitaxel in vivo via regulation of the expression of UPR-related miRNAs.

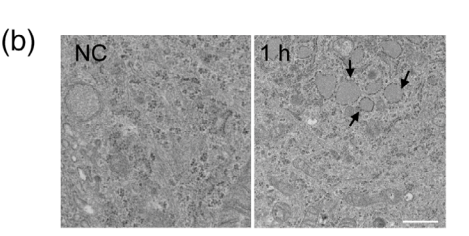
2 | RESULTS

2.1 | *U. parvum* induced reactive oxygen species but terminated the downstream ER stress cascade

We examined the colocalization of intracellular *U. parvum* and host cellular organelles. Fluorescent microscopic observations revealed that *U. parvum* colocalized with ER (Figure 1a). After 1 hr of *U. parvum* infection in HeLa cells, an electron micrograph showed that the ER had swollen into a round structure, indicating that ultrastructural changes due to ER stress were initiated (Figure 1b). In order to

FIGURE 1 U. parvum infection of HeLa cells induces ER stress. (a) HeLa cells stably expressing ER-EGFP were infected with Dil-labelled U. parvum for 3 hr. The left lower corner white inset showed the magnified image of the central white box in the Merged image. Scale bar: 10 µm. (b) Transmission electron microscopy images of uninfected HeLa cells (negative control; NC) or infected with U. parvum for 1 hr. Black arrow indicates ER swelling. Scale bar: 200 nm. (c) Detection of ER stress proteins (BiP, IRE1α, PERK, P-eIF2 α , eIF2 α , CHOP, ATF4. XBP1) in U. parvum-infected or uninfected and BFA-treated (as a positive control) HeLa cells for 3-24 hr





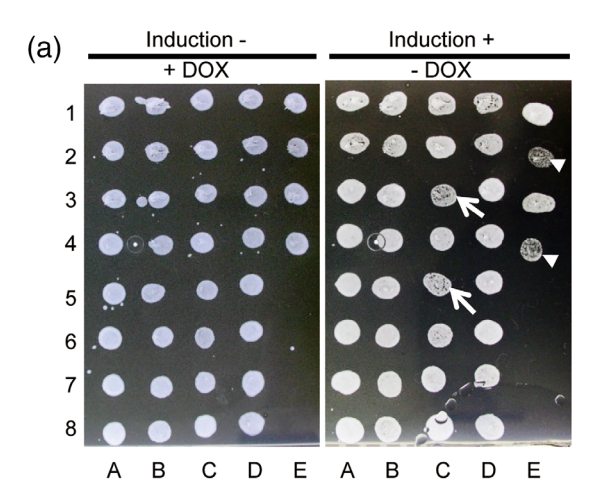
elucidate the mechanisms underlying U. parvum-induced ER stress, the protein levels of various ER stress markers in HeLa cells were analysed by western blotting. The expression levels of the upstream ER stress markers BiP. PERK. P-elF2α and IRE1α were increased 3-24 hr after infection in a time-dependent manner. Interestingly, the downstream ER stress markers ATF4, XBP1 and CHOP were almost undetectable in *U. parvum-*infected HeLa cells contrasting with brefeldin A (BFA), an ER stress inducer. BFA induced both upstream and downstream ER stress markers in HeLa cells (Figures 1c and S1a). Our data suggest that U. parvum infection damaged intracellular organelles and initiated the activation of BiP, PERK, P-eIF2 α and IRE 1α , but not the downstream ER stress cascade. Next, we examined the production of ROS in HeLa cells, monitored by a CellROX, 3 hr after U. parvum infection (Figure S1b-c). Production of ROS was significantly higher in U. parvum-infected HeLa cells than in uninfected HeLa cells (***p < 0.0001) (Figure S1c). Electron micrograph of U. parvum-infected HeLa cells showed swollen mitochondria, and their cristae were disrupted after 3 hr of infection (Figure S1d).

GAPDH

2.2 | Screening of *U. parvum* pathogenic effector involved in intracellular organelle damage

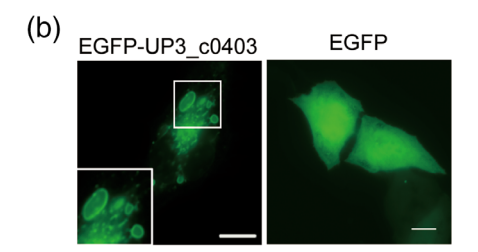
Mycoplasmas use the TGA codon as a tryptophan coding codon. Because of this, genes with TGA codons cannot be PCR cloned from mycoplasma genomic DNA and then expressed in vector systems that use the standard genetic code because the mycoplasma TGA codons

would be read as translational stop codons. Expression of mycoplasma genes containing TGA codons in organisms such as yeast or Escherichia coli requires resynthesis using the standard genetic code or mutagenesis to convert those codons to TGG. For this project, we were unable to undertake resynthesis of hundreds of U. parvum genes; however, we were able to experiment with *U. parvum* genes that did not have TGA codons or that had TGA codons that could be mutated using mutagenic PCR primers. From the deduced hypothetical proteins encoded by the U. parvum SV3F4 genome (GenBank accession no. AP014584.1), we selected 31 genes for a yeast expression screening system: 30 genes that did not contain TGA codons and 1 gene that includes a single TGA codon at the C-terminus (amino acid position 264 among 286 residues) (UP3_c0231) (Table S1). The retransformation of yeast cells confirmed the inhibitory effect of the selected ureaplasmal genes on yeast growth. Two genes, UP3_c0403 (corresponding to UU334 gene of U. parvum serovar 3 str. ATCC 700970: GenBank accession no. AF222894.1) and UP3_c0420 (corresponding to the UU319 gene of ATCC 700970 strain), were detected as novel virulence factor genes based on their expression. UP3_c0403 inhibited yeast growth more strongly than UP3_c0420 but not as much as a positive control Yersinia enterocolitica YpkA or Salmonella typhimurium SopE2 (Figures 2a and S2a). Y. enterocolitica effectors (YpkA, protein kinase) and S. typhimurium effectors (SopE2, Rho-GEF) were growth inhibitory phenotypes on yeast (Lesser & Miller, 2001; Rodriguez-Escudero, Rotger, Cid, & Molina, 2006; Rodriguez-Pachon et al., 2002; Tabuchi et al., 2009). We focused on upr: UP3_c0403, the product of UP3_c0403 gene, which has a



	Α	В	С	D	E
1	*Up-F4-r2	<i>Up</i> 3_c0225	<i>Up</i> 3_c0364	<i>U</i> p3_c0471	empty
2	Up3 c0038	Up3_c0231	Up3_c0385	Up3_c0530	SopE2
3	Up3_c0049	Up3_c0246	Up3_c0403	Up3_c0535	empty
4	Up3_c0070	Up3_c0275	Up3_c0413	Up3_c0546	YpkA
5	Up3_c0086	Up3_c0311	Up3_c0420	Up3_c0558	
6	Up3_c0094	Up3_c0319	Up3_c0426	Up3_c0559	
7	Up3_c0144	Up3_c0338	Up3_c0438	Up3_c0561	
8	Up3_c0156	Up3_c0349	Up3_c0445	Up3_c0566	

*Up-F4-r2 encodes 23S rRNA gene.



candidate confers a growth inhibitory phenotype in yeast. (a) Upper images, 32 U. parvum genes were expressed in yeast cells under the control of a Tet-Off promoter. Yeast strains carrying Tet-Off promoter plasmids were cultured in SC-Ura/glucose with 20 µg/mL doxycycline, and cells in the exponential growth phase were washed with the same medium without doxycycline and spotted in 10-fold serial dilution on SC-Ura/fructose with and without doxycycline. The white arrows show the growth inhibitory phenotype. Arrowheads showed yeast growth inhibition caused by SopE2 and YpkA as control. The lower list, the deduced ORF number of U. parvum SV3F4 genes (GenBank: AP014584.1), is expressed in the yeast vesicular trafficking screening system. (b) EGFP was monitored after 24 hr post-transfection of pEGFP-C1 or pEGFP-UP3_c0403 in HeLa cells. The large membranous vacuolation was magnified in the white box of the left lower corner. Scale bar: 10 µm

FIGURE 2 Pathogen protein

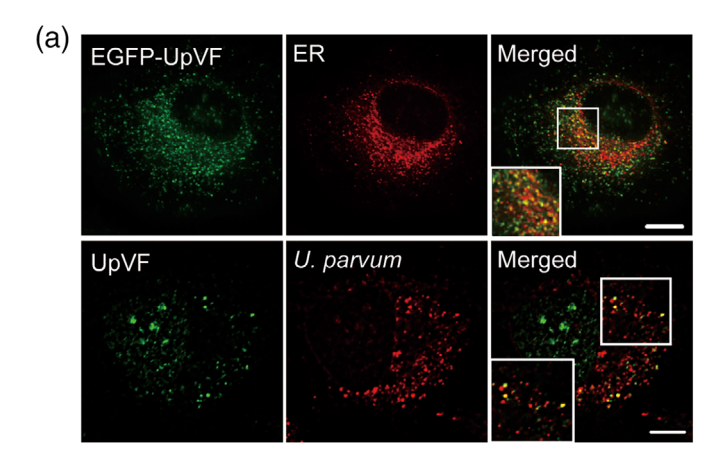
deduced molecular mass of 9.6 kDa. In order to examine its cytotoxicity, enhanced green fluorescent protein (EGFP)-tagged upr: $UP3_c0403$ was expressed in HeLa cells. The transient expression of EGFP-tagged $UP3_c0403$ significantly decreased cell viability (64.6% \pm 6.0%) compared with EGFP mock transfection (90.7% \pm 4.7%) (Figure S2b, p < 0.001). By the fluorescence microscopic observations, EGFP-tagged $UP3_c0403$ expression resulted in large vacuoles in the cytoplasm of HeLa cells (Figure 2b). Therefore, we named gene upr: $UP3_c0403$ U. parvum vacuolating factor (UpVF). Analysis of the UpVF sequence showed it was only similar to genes in other ureaplasmas, including ureaplasma species that infect non-human animals. It is present in all ureaplasma genomes.

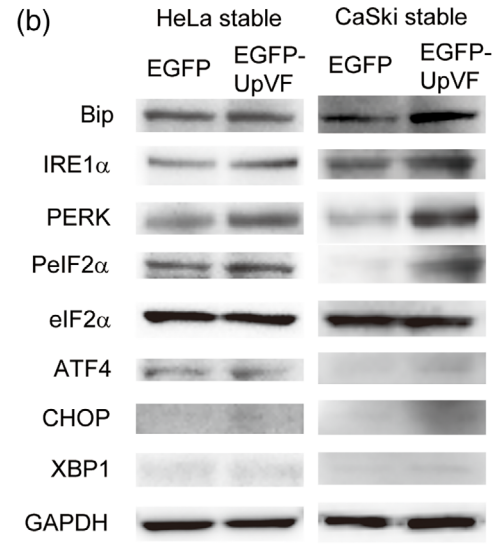
2.3 | UpVF inhibited downstream ER stress markers and affected miRNA profiles

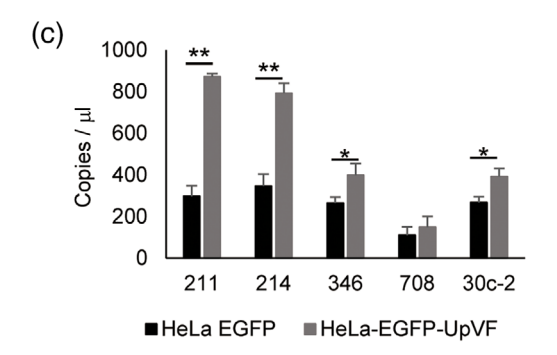
Although the transient overexpression of UpVF caused HeLa cell death (Figure 2b), we succeeded in establishing cell lines that stably expressed EGFP-UpVF. The expressed EGFP-UpVF colocalized

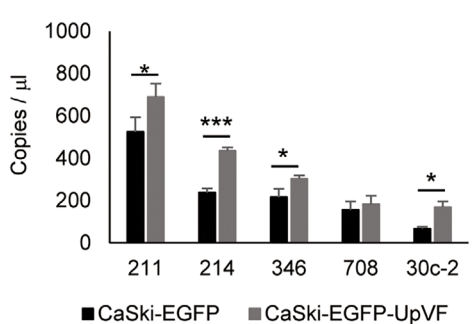
with the ER in HeLa cells (upper), and colocalization of UpVF with Dil-labelled U. parvum-infected cells (lower) (Figure 3a). Stably expressed EGFP-UpVF cells reached the same proliferation rate of HeLa cells at 8 days, while CaSki cells showed faster proliferation than EGFP cells at 6 days (Figure S3a-b). However, the growth of U. parvum-infected cells was slower than uninfected cells (Figure S3c). In order to clarify the association between UpVF and the ER stress cascade, we performed western blot analyses to quantify the ER stress markers and found that stable expression of EGFP-UpVF increased the expression of the upstream markers BiP, IRE 1α , PERK and P-eIF 2α , but downstream markers, including ATF4, CHOP and XBP1 (Figures 3b and S3d), were not increased in HeLa and CaSki stably expression cells. On the other hand, transient expression of EGFP-UpVF increased the expression of the upstream markers BiP, IRE1PERK and P-eIF2, and the downstream marker ATF4, but not CHOP or XBP1, in HeLa and CaSki cells (Figure S3e). The overexpression of UpVF may induce ER stress more intensely than during *U. parvum* infection. These observations correspond to the profile of the ER stress markers of U. parvuminfected HeLa cells.

FIGURE 3 Analysis of UpVF function. (a) Upper images, HeLa cells stably expressing EGFP-UpVF were stained with anticalreticulin-ER marker, followed by Alexa 568 secondary antibody. Lower images, HeLa cells were infected with Dillabelled (red) U. parvum for 3 hr. U. parvum was detected with anti-UpVF (44-53) antibody (green). The merged image was magnified in the white box of the left lower corner. Scale bar: 10 μm. (b) ER stress proteins detected by western blot with control HeLa and CaSki cells stably expressing EGFP or stably expressing EGFP-UpVF were Bip, IRE1 α , PERK, P-eIF2 α , eIF2α, ATF4, CHOP and XBP1. GAPDH was measured as a loading control. (c) Analysis of ER stress-related miRNA expression in EGFP- or EGFP-UpVFexpressing HeLa and CaSki cells. p < 0.05, **p < 0.005,***p < 0.0005 compared with EGFP-UpVF









Next, comparative microarray analyses, including 2,578 human miRNAs, were performed to determine miRNA levels in *U. parvum*-infected and uninfected (WT) HeLa cells. Eighty-two differentially expressed miRNAs were identified when the two HeLa cell samples were compared (Figure S3f). Among ER stress-related miRNAs, a total of five upregulated miRNAs were identified as follows: miR-214-5p, -211-5p, -34b-5p, -122-3p and -140-5p. A further 20 miRNAs were downregulated during infection (Figure 3c). Next, in order to compare the profile of miRNAs known to be upregulated during ER stress between cells stably expressing EGFP-UpVF (HeLa and CaSki cells) and control EGFP-expressing cells, digital PCR analyses were performed. Among five miRNAs regulating the ER stress cascade

(miR-211, -214, -346, -708 and -30c-2*), four (miR-211, -214, -346 and -30c-2*) were upregulated in both UpVF-expressing HeLa and CaSki cells (Figure S3g). Because miR-211 and miR-214 were upregulated in both *U. parvum*-infected cells and UpVF-expressing cells, these results led us to hypothesise that miR-211 and miR-214 are indispensable for terminating the ER stress cascade. On the other hand, the miR-211, -214 levels were decreased in BFA-treated cells compared with UpVF-expressing cells (Figure S3h). Thus, the induction of apoptosis occurred in the BFA-treated cells. We, therefore, used a miRNA inhibitor to suppress miR-211 or miR-214 in EGFP-UpVF cells. These miR-211 or -214 specific inhibitors activated apoptotic cascade by western blotting and transferase dUTP nick-end

labelling (TUNEL) assays. As shown in Figure 4a, cleaved PARP and caspase 3 were increased in cells transfected with miR-211 and miR-214 inhibitors (Figure S4a). To confirm the effect of mimics of miR-211 and miR-214 upon ER stress induced by BFA, CHOP was quantified. Both miR-211 and -214 mimics downregulated the protein level of CHOP after BFA treatment in HeLa and CaSki cells (Figure S4b,c).

These results corresponded to the suppression of CHOP after *U. parvum* infection and the expression of UpVF in vitro (Figures 1c and 3b). The percentage of TUNEL-positive cells significantly increased after miR-211 or miR-214 inhibitor transfection (Figure 4b, c). These results confirm that UpVF-expressing cells had the potential to suppress apoptosis. In UpVF-expressing cell lines, the downstream

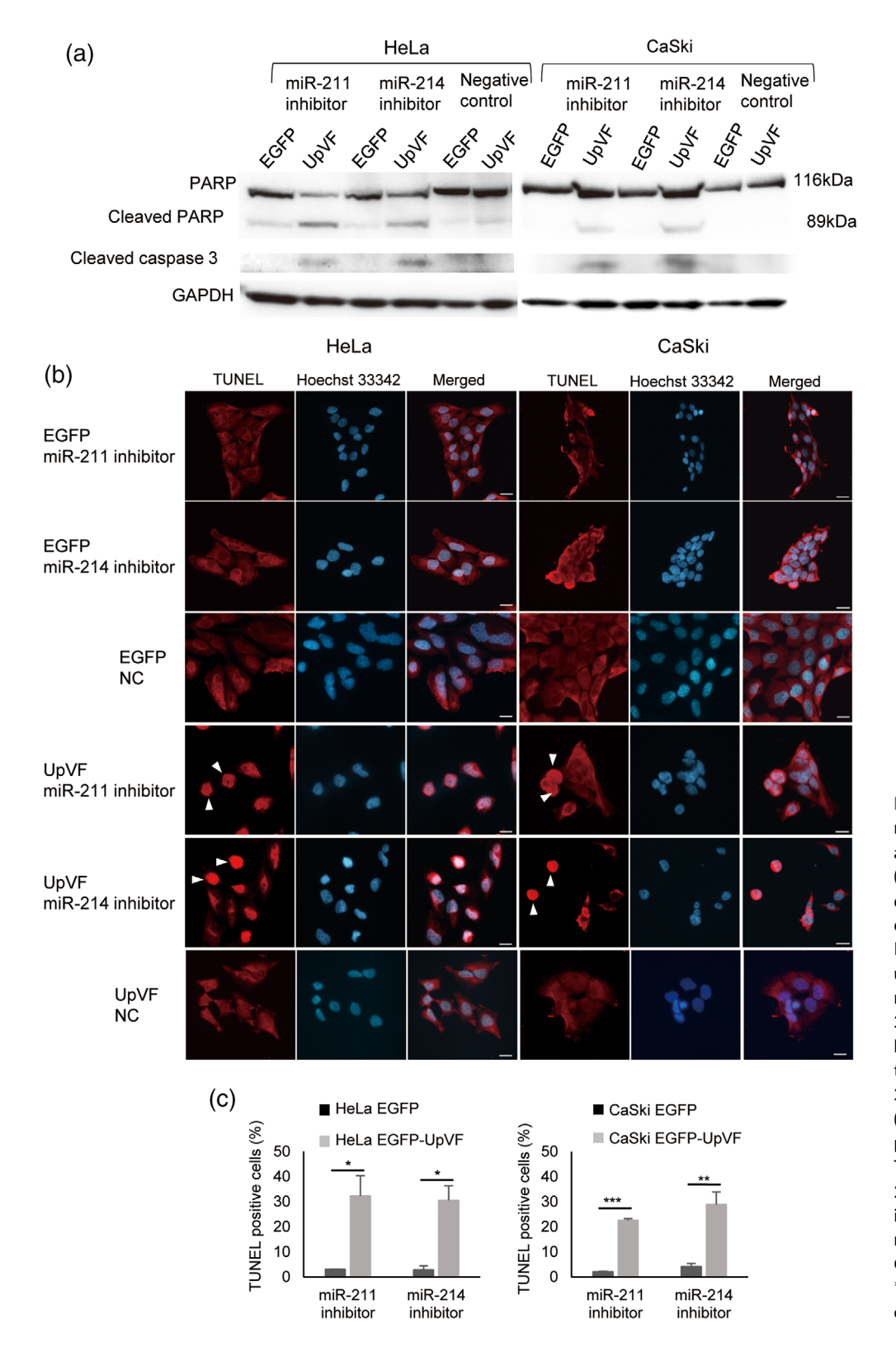


FIGURE 4 Knockdown of miR-211 and miR-214 induced apoptosis in EGFP-UpVF cells. (a) Western blotting was used to detect PARP, cleaved PARP and cleaved caspase 3 in EGFP and EGFP-UpVF HeLa and CaSki cells under miR-control, miR-211 and miR-214 inhibitor transfection for 24 hr. GAPDH was used as a loading control. (b) Cells were transfected with miR-211, miR-214 inhibitor or negative control (NC), and TUNEL staining was performed. Arrowhead showed TUNEL-positive cells. Scale bar: $20 \mu m.$ (c) miR-211 or miR-214 inhibitor raised the apoptotic cell ratio in UpVF expressed HeLa or CaSki cells. (*p < 0.05, **p < 0.005, ***p < 0.0005compared with EGFP)

ER stress cascade was diminished via the upregulation of miR-211 and miR-214.

2.4 | Stable UpVF expression confers protection against irradiation and anticancer drugs in cervical cancer cells

In this study, we demonstrated the inhibition of apoptosis in UpVF-expressing cells. We investigated the resistance of *U. parvum*-infected and UpVF-expressing cells of the cervical cancer cell lines HeLa and CaSki to various anticancer agents, including two DNA-binding agents

(actinomycin D and cisplatin) and one tubulin-targeting drug (paclitaxel). Cisplatin and paclitaxel are clinically used in anticancer chemotherapy for patients with cervical cancer. It was found that both agents led to apoptosis. We first performed cell viability assays. After treatment with 0.5 μM actinomycin D, the viability of *U. parvum*-infected (MOI 10) cells was 1.3 and 1.2 times higher than that of control HeLa and CaSki cells, respectively (Figure 5a). Next, we used EGFP-UpVF-stable transformant HeLa and CaSki cell lines for cell viability assays to determine the effect of UpVF on drug resistance. We observed that EGFP-UpVF-expressing cells were more resistant to actinomycin D (Figure 5b), similar to *U. parvum*-infected cells. The cell viability of HeLa-EGFP cells treated with cisplatin was approximately

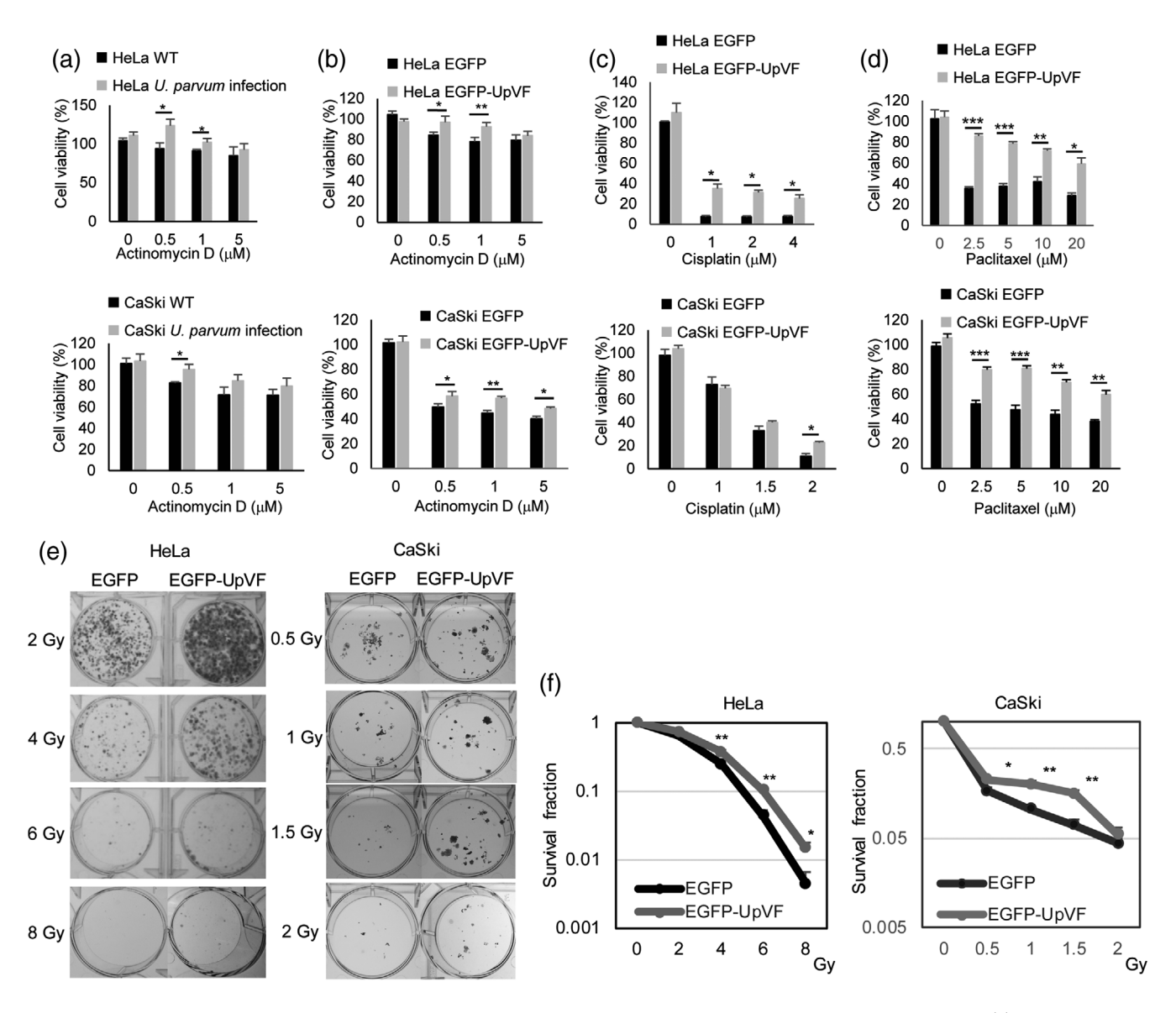


FIGURE 5 *U. parvum*-infected or EGFP-UpVF-expressing cervical cancer cells were highly resistant to anticancer agents. (a) Cell viability in *U. parvum*-infected and WT cells (HeLa and CaSki) treated with actinomycin D for 6 hr. *p < 0.05 compared with *U. parvum* infection. (b) Cell viability in EGFP- or EGFP-UpVF-expressing HeLa and CaSki cells treated with actinomycin D for 6 hr. *p < 0.05, *p < 0.005 compared with EGFP-UpVF. (c),(d) Cell viability in EGFP- or EGFP-UpVF-expressing HeLa and CaSki cells treated with cisplatin (c) or paclitaxel (d) for 24 hr. *p < 0.005, *p < 0.005, *p < 0.0005 compared with EGFP-UpVF. (e) The colony formation of different cells under X-ray radiation was examined. Colonies of cells stably expressing EGFP or EGFP-UpVF were stained with 0.5% crystal violet. (f) Survival of different cells under different doses of X-ray radiation (HeLa, 2–8 Gy; CaSki, 0.5–2 Gy). *p < 0.005 compared with EGFP-UpVF

7% at any dose tested (Figure 5c). Conversely, HeLa-EGFP-UpVF cells showed 3.4-4.6 times higher cell viability (25-34%, *p < 0.05) when treated with cisplatin. CaSki cells showed a dose-dependent response to cisplatin and were more resistant to cisplatin than were HeLa cells. When 2 µM cisplatin was administered to CaSki-EGFP cells, cell viability decreased to 11%. The cell viability of HeLa-EGFP-UpVF cells was significantly higher than that of HeLa-EGFP cells at the concentrations of 1-4 µM of cisplatin. On the contrary, CaSki-EGFP-UpVF cells showed resistance to cisplatin at $2 \mu M$ (Figure 5c). On the other hand, the addition of 2.5–20 µM paclitaxel, UpVF was advantageous for cell survival in both HeLa and CaSki cells (Figure 5d). HeLa and CaSki cells stably expressing UpVF were approximately 2 and 1.5 times, respectively, more resistant to paclitaxel than control cells. Furthermore, we investigated the proliferation of cells after 2, 4, and 6 days of treatment with 2.5 µM paclitaxel or 1 µg/mL BFA, which indicated that cells stably expressing UpVF proliferated more than control cells (Figure S5a). Stable expression of EGFP-UpVF in HeLa and CaSki cells suppressed cleaved caspase 3 protein level induced after cisplatin and paclitaxel treatment compared with the EGFP expressed group (Figure S5b). To further validate the role of UpVF in resistance to cancer therapies, the radioresistance of EGFP-UpVF-stable transformant HeLa and CaSki cells was evaluated. HeLa cells were irradiated with X-rays at 2, 4, and 8 Gy, and CaSki cells were irradiated at 0.5, 1, 1.5, and 2 Gy. Then, the cells were tested for colony formation. As shown in Figure 5e.f. the number of colonies formed after 10 days was significantly higher in HeLa and CaSki cells expressing EGFP-UpVF. The survival rates of HeLa expressing MOCK EGFP compared with those expressing EGFP-UpVF under various amounts of radiation were as follows: 2 Gy, 64% and 73.6%; 4 Gy, 24.4% and 37%; 6 Gy, 4.3% and 10.2%; and 8 Gv. 0.4% and 1.4%, respectively. For CaSki cells, the results were as follows: 0.5 Gy, 17% and 22.8%; 1 Gy, 10.6% and 20.1%; 1.5 Gy, 4.3% and 5.5%; and 2 Gy, 0% and 0.3%, respectively. These results confirm that EGFP-UpVF induced radioresistance and chemoresistance in HeLa and CaSki cells.

2.5 | Syn-MBA-UpVF induced cell membrane permeability

We utilised near minimal bacterium JCVI-syn3A (GenBank CP016816.2) harbouring the minimal synthetic *Mycoplasma mycoides* genome and JCVI-syn3B harbouring *dual loxP* landing pad in the JCVI-syn3A genome (Hossain, Deter, Peters, & Butzin, 2021; Pelletier et al., 2020) as a mycoplasma vehicle to express *U. parvum* surface membrane lipoprotein multiple banded antigen (MBA) and UpVF. MBA with 24 six-amino acid repeats at the C-terminus (GenBank accession no. LC604071) was selected by PCR amplification to create expression plasmid based on the MBA of SV3F4 (GenBank accession no. AP014584.1, *UP3_c0361*). Two expression plasmids, pSyn-MBA and pSyn-MBA-UpVF, were constructed (Figure S6a,b), and JCVI-syn3B cells were transformed with these plasmids to produce Syn-MBA and Syn-MBA-UpVF strains, respectively. The Syn-MBA strain was designed to express the MBA, and the Syn-MBA-UpVF strain

was designed to express both MBA and UpVF. As shown in Figure S6c, western blotting with antibodies against MBA and UpVF revealed that the mycoplasma cells expressed an MBA and UpVF. Whereas JCVI-syn3B did not attach to HeLa cells (Figures 6a and S6d). After 6 hr of infection, Syn-MBA and Syn-MBA-UpVF attached to HeLa cells in contrast to JCVI-Syn-3B by fluorescent microscopic observation (Figure 6a) or low vacuum scanning electron microscopy (SEM) (Figure S6d). These data indicate that MBA was essential for host cellular attachment.

The uptake of propidium iodide (PI) was monitored after 6 hr of infection. By calculating the ratio of PI-positive/MBA-positive HeLa cells, Syn-MBA-UpVF significantly increased HeLa cell membrane permeability towards cell death (67.9% \pm 3.7%, n=5) when compared with that of Syn-MBA (33.7% \pm 3.5%, n=5, p<0.0005) (Figure 6b). These findings indicated that the Syn-MBA-UpVF induced relative acute HeLa cell deaths. We identified an association between Syn-MBA- or Syn-UpVF-induced ER stress, and the protein levels of various ER stress markers in HeLa cells were analysed by western blotting. JCVI-syn3B, Syn3-MBA and Syn3-MBA-UpVF increased the expression of the upstream markers PERK and P-eIF2 α of HeLa cells at 6–24 hr after infection, but did not increase downstream markers (ATF4 and XBP1). Interestingly, after 24 hr of Syn3-MBA-UpVF infection in HeLa cells, the ER stress marker P-eIF2 α was decreased (Figure S6e).

We further quantified MBA-positive HeLa cell counts after 24, 48 and 72 hr of infection. The infected MBA-positive HeLa cell counts were as follows: Syn-MBA (12.3 \pm 2.0, n=3 microscopic field) and Syn-MBA-UpVF (15.3 \pm 2.1, n=3) at 24 hr; Syn-MBA (14.3 \pm 4.0, n=3) and Syn-MBA-UpVF (17.0 \pm 6.0, n=3) at 48 hr, respectively (p=0.98, and p=0.93, respectively). The HeLa cell counts did not show significant differences between Syn-MBA or Syn-MBA-UpVF infection at 24 and 48 hr. On the contrary, HeLa cell counts were significantly increased after infection of Syn-MBA-UpVF (42.6 \pm 2.1, n=3) at 72 hr, while Syn-MBA (7.6 \pm 3.1, n=3) infected HeLa cells did not (p < 0.0005) (Figure 6c). These results together indicated that longer time exposure (72 hr) of UpVF enhanced the survival of infected HeLa cells.

2.6 | Xenograft tumour growth assay

To determine whether UpVF affects resistance to chemotherapy in vivo, we performed a xenograft assay. As shown in Figure 7a, we injected EGFP or EGFP-UpVF-stable transformant CaSki cells subcutaneously into nude mice. After the volumes of the resulting tumours reached approximately 100 mm³, mice were treated by i.p. injection with vehicle or anticancer drugs. Cisplatin was administered twice at a final concentration of 7 mg/kg each. Paclitaxel was administered at a final concentration of 12 mg/kg every other day. Once the mice were sacrificed at the endpoint of the experiment, the histological features of the tumours were evaluated. As shown in Figure 7b (left panel), mice with EGFP tumours treated with cisplatin showed significantly higher long-term survival than the vehicle treatment groups (26 days

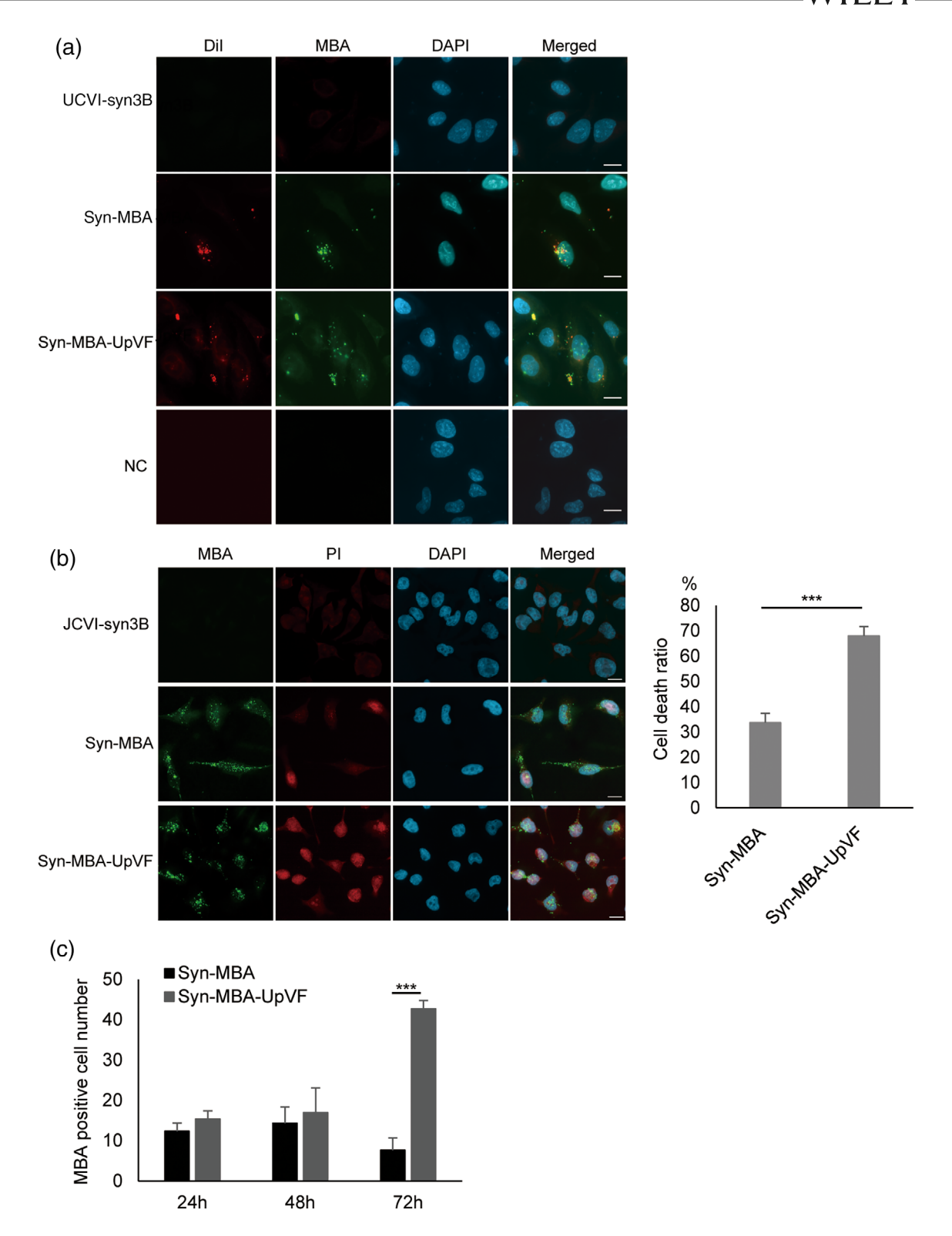


FIGURE 6 Syn-MBA- and Syn-MBA-UpVF-induced cell damage. (a) HeLa cells were infected with Dil-labelled JCVI-syn3B, Syn-MBA, Syn-MBA-UpVF or uninfected (negative control; NC) for 6 hr. MBA (green), Propidium Iodide (PI, red), DAPI (blue). Scale bar: 10 μ m. (b) Quantification of HeLa cell membrane permeability induced by Syn-MBA or Syn-MBA-UpVF. The HeLa cells were infected with JCVI-Syn-3.0, Syn-MBA or Syn-MBA-UpVF for 6 hr. MBA (green), PI (red) and DAPI (blue). Scale bar: 10 μ m. PI-positive HeLa cells were counted as the dead cells. (n=6 microscopic field, ****p < 0.0001 compared with Syn-MBA-UpVF). (c) HeLa cells were infected with Syn-MBA or Syn-MBA-UpVF for 24, 48 and 72 hr. Quantification of MBA-positive HeLa cell counts of Syn-MBA or Syn-MBA-UpVF (mean \pm SEM, n=3 microscopic field, ****p < 0.0005 compared with Syn-MBA-UpVF)

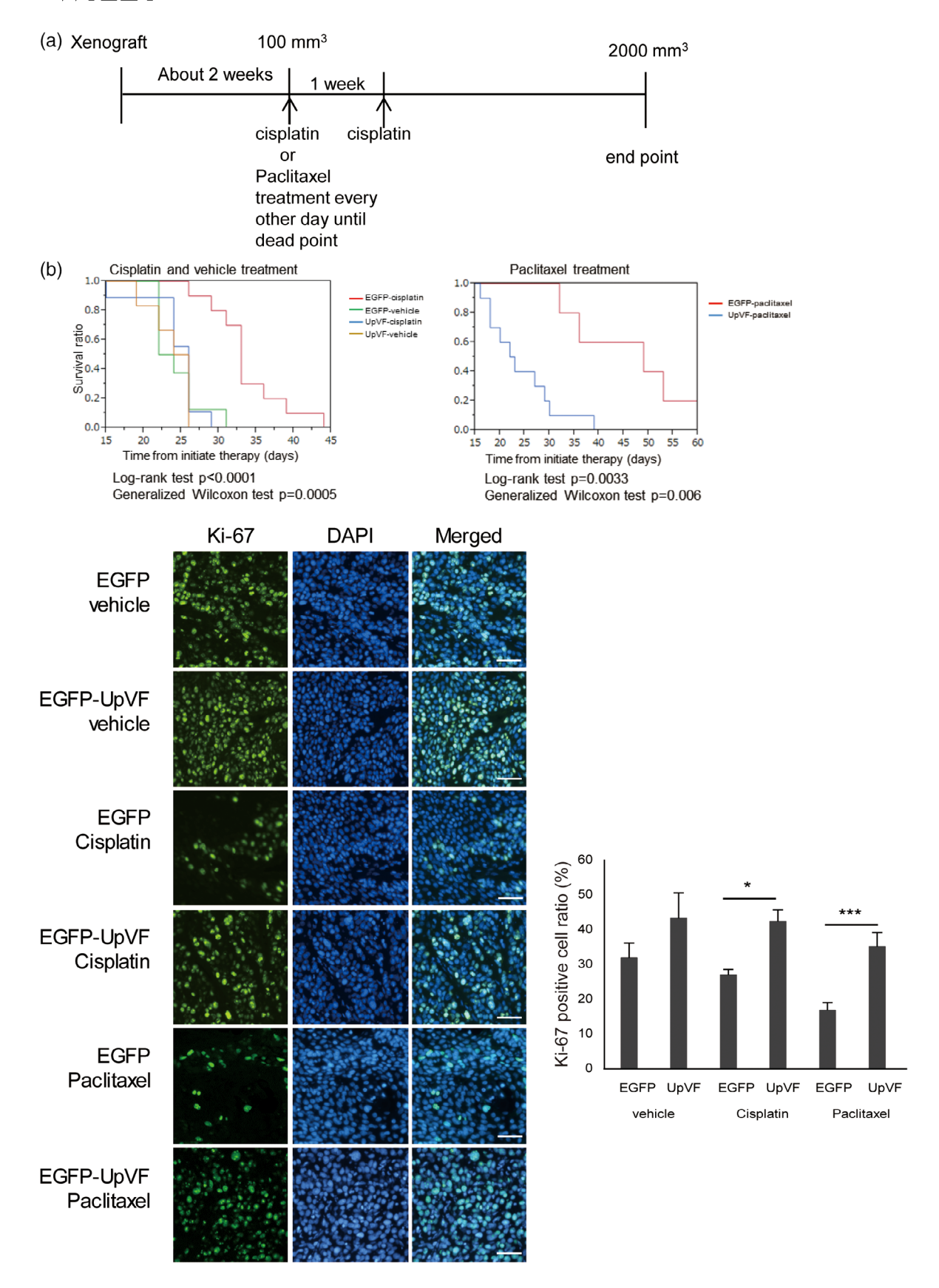


FIGURE 7 Nude mouse xenograft. (a) Treatment regimen for tumour cell xenograft models (EGFP- or EGFP-UpVF-expressing cells). (b) The survival (Kaplan-Meier) curves of treated animals are shown. Prolonged survival was observed in the cisplatin or paclitaxel treatment group as compared with the vehicle group. (Left panel) EGFP- cisplatin, n = 10; UpVF-cisplatin, n = 9; EGFP-vehicle, n = 8; UpVF-vehicle n = 6. (Right panel) EGFP-paclitaxel, n = 5; UpVF-paclitaxel, n = 10). (c) Analysis of mitotic status by Ki-67 staining of tumour cell xenografts in vivo (EGFP- or EGFP-UpVF-expressing cells) after vehicle, cisplatin and paclitaxel treatment. Representative Ki-67 immunostaining images are presented on the left. Scale bar: 50 μ m. Percentages of Ki-67-positive cells in tumour cell xenografts (EGFP- or EGFP-UpVF-expressing cells) after vehicle, cisplatin (7 mg/kg) or paclitaxel (12 mg/kg) treatments are shown on the right. (mean \pm SEM, n = 200 cells; *p < 0.05 compared with UpVF-cisplatin treatment, ****p < 0.0005 compared with UpVF paclitaxel treatment)

vs. 44 days). In contrast, cisplatin did not affect the survival of mice with xenograft EGFP-UpVF-stable transformant cells (endpoint: day 26). Similarly, mice in the EGFP-UpVF-stable transformant cell xenograft group that received paclitaxel died earlier than those in the EGFP-stable transformant cell xenograft group (39 days vs. >60 days) (Figure 7b, right panel). Histological analyses revealed that compared with EGFP-UpVF transformant tumours, treatment of EGFP transformant tumours with cisplatin and paclitaxel decreased expression of the proliferation marker Ki-67 (Figure 7c). These results indicate that the EGFP-UpVF conferred resistance to anticancer drug chemotherapy in vivo.

3 | DISCUSSION

Since the first report of mycoplasma in cancer tissue in the 1960s, various mycoplasma species have been found to co-exist with neoplasms (Tsai, Wear, Shih, & Lo, 1995). Additionally, the 1,000 Genome Project reported that 7% of the samples included mycoplasma DNA (Olarerin-George & Hogenesch, 2015). To date, 35 *U. urealyticum* and *U. parvum* whole-genome sequences have been deposited in the NCBI genome database (https://www.ncbi.nlm.nih.gov/genome/). Among them, 13 genomes possess upr: *UP3_c0403* homologues, including four genomes from *U. parvum* serovar 3 and 1 genome from *U. urealyticum* serovar 10 (Figure S7). *U. parvum* serovar 3 is one of the most frequently isolated ureaplasma serotypes: 66 strains (28.4%) from 232 *Ureaplasma* spp. (Payne et al., 2016) and 540 strains (43.3%) from 1,247 *U. parvum* clinical isolates (Rittenschober-Bohm et al., 2019) obtained from women of child-bearing age. It is necessary to confirm the expression of UpVF in many clinical isolates in the future.

TGA is a stop codon in most organisms. In contrast, TGA codon encodes tryptophan in ureaplasmas and many mycoplasmas (Dybvig & Voelker, 1996). This TGA codon problem makes it difficult to construct a high-throughput expression system of *Ureaplasma* recombinant proteins in eukaryotic cells. Therefore, we did not screen all of the 232 unassigned genes in the yeast screening assay but selected 31 genes of unassigned 28 genes and 3 genes with possible assigned functions (Table S3). Among these 31 genes, 30 genes did not include TGA codon, and only *UP3_c0231* gene had a single TGA codon near the C-terminus. Based on the yeast functional assay results, two candidate genes, *UP3_c0403* and – 420, were discovered to encode proteins involved in membrane damage. Given the inhibitory effects on yeast growth (Figure 2), we further focused on *UP3_c0403* (Figure S3) and its encoded product UpVF.

Ideally, we would have tested *U. parvum* mutants lacking *UpVF* to see whether they caused the cytopathic effects in yeast and mammalian cells. Unfortunately, there are no methods available at present for the genetic manipulation of *U. parvum* SV3F4. Instead, we chose to install *UpVF* in a different genetically malleable mycoplasma. JCVI-syn3B is a derivative of the near minimal bacterial cell JCVI-syn3.0 (CP014940). This organism's synthetic genome was designed to encode only a minimal set of essential genes that are necessary for life (it still contains a small number of non-essential genes). It is a

derivative of M. mycoides subspecies mycoides strain GM12. Considering that the genome of JCVI-syn3.0 is chemically synthesised, its genome can be altered in any way that can yield a viable cell. JCVIsyn3A (CPO16816) and JCVI-syn3B (Pelletier et al., 2020) are the variants of the minimal cell JCVI-syn3.0 that contain an additional 19 genes that make the cell morphology more stable and working with bacteria easier. JCVI-syn3B contains an additional dual loxP landing pad that enables direct insertion of a new DNA between the loxP sites in a Cre recombinase-mediated reaction. We have conducted studies in the past that showed none of the three minimal cell variants (i.e., syn3.0, syn3A, and syn3B) were capable of infecting mammalian cell cultures. Unlike the wild-type M. mycoides, which attach to and replicates in all cultured cells tested, within 1 week of being mixed with HeLa cells, all the minimal cells die (manuscript in preparation). We hypothesised a JCVI-syn3B strain expressing the U. parvum serovar 3 mba, which has been proposed as an attachment protein gene (Monecke, Helbig, & Jacobs, 2003), could attach to and infect HeLa cells. This organism, which we termed Syn-MBA, was confirmed to infect HeLa cells. Next, we prepared Syn-MBA-UpVF, a JCVI-syn3B strain that expressed both MBA and UpVF. We reasoned that this organism could serve as a surrogate to deliver the UpVF to mammalian cells and that Syn-MBA could serve as a negative control. As expected, we observed that JCVI-syn3B failed to attach to HeLa cells. In contrast, both of JCVI-svn3B-derived strains expressing U. parvum MBA (Svn-MBA) and MBA plus UpVF (Svn-MBA-UpVF) were capable of attaching to HeLa cells (Figure 6a). The cytotoxicity of HeLa cells was significantly higher in Syn-MBA-UpVF infection than in Syn-MBA infection after 6 hr (Figure 6b). Syn-MBA and Syn-MBA-UpVF infection reduced the number of HeLa cells after 24 hr of infection compared with JCVI-syn3B. However, at 72 hr after infection, the survival rate of Syn-MBA-UpVF-infected HeLa cells was higher than Syn-MBA-infected cells, indicating that UpVF would inhibit cell death at 72 hr (Figure 6c). These results are consistent with the transient expression of UpVF in HeLa cells (Figure 2b) and stable transformant analyses (Figure 3). From these data, overexpressed or unregulated expression of UpVF seems to act as a celldamaging virulence factor at the initial step of the infection. However, once the infected host cells survive, those host cells gain the escape mechanism of cell death. We also speculate the MBA has a certain HeLa cell toxicity, and UpVF would reduce the MBA-induced host cell toxicity at least at 72 hr of infection, which recovered the host cell survival.

UpVF damages intracellular organelles and the transient expression of UpVF leads to the formation of large vacuoles in HeLa cells (Figure 2b). Ureaplasmas and mycoplasmas have evolved by reducing the size of their genomes, resulting in a limited biosynthesis capability that requires the intake of various nutrients from their host as amino acids, cholesterol, fatty acids and nucleic acid precursors. Previously, we reported that ureaplasma disrupts the endocytic membrane system of host cells (Nishiumi et al., 2017). In this paper, we isolated UpVF as a molecule that disrupts the host cell membrane system. Within 3 hr of *U. parvum* infection, ROS production was induced and colocalized with ER in HeLa cells.

Bacterial infections modulate subcellular organelles, such as mitochondria and the ER, which generate ROS (Paiva & Bozza, 2014; To et al., 2020). ER stress and mitochondrial fragmentation induce ROS production (Lee & Song, 2021). Oxidative stress is closely related to ER stress during pathogen infection and triggers the production of proinflammatory cytokines, generation of ROS, autophagy and apoptosis (Bischof et al., 2008; Loose et al., 2015; Pillich, Loose, Zimmer, & Chakraborty, 2016). We previously reported that U. parvum leads to ROS production in HEK293T cells, mouse macrophages (Wakimoto et al., 2015) and mouse sperm (Ito et al., 2021). NAC (N-acetyl-L-cysteine) inhibits ROS-dependent apoptosis (Curtin, Donovan, & Cotter, 2002). ROS scavengers, including NAC, are commonly used to confirm the involvement of ROS in drug-induced apoptosis. To examine the relationship between ROS production and UpVF-vacuole formation. NAC was treated before transient transfection with EGFP or EGFP-UpVF. UpVF stably expressing cells, ROS production was not higher than in *U. parvum*-infected cells (Figure S1e). Still, the vacuole formation ratio was diminished after the inhibition of ROS production by NAC (Figure S1f,g). Our results suggest that ROS production was involved in the vacuolization process, whether the effect is direct or indirect. To clarify the precise mechanisms underlying the UpVFinduced vacuolization, a future study will be needed.

This study demonstrated that ER stress is induced in cervical cancer cells infected with U. parvum. ER stress sensors, such as PERK and IRE1 α , may be activated in such conditions. Both miR-211 and miR-214 were shown to be induced by U. parvum infection in a PERK- and eIF2 α -dependent manner (Figure 8). Both miR-211 and -214 have been demonstrated to be dysregulated in various cancers and shown to govern both tumorigenic and tumour-suppressive characteristics (Sharma, Hamilton, & Mandal, 2015). Additionally, miR-211 and -214

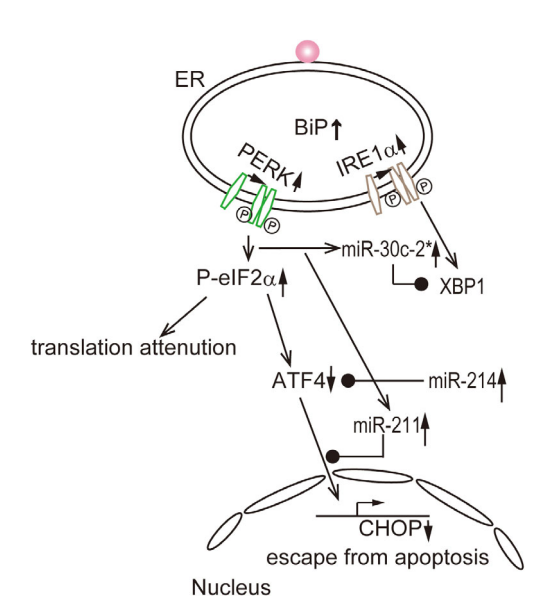


FIGURE 8 Illustration of miRNA and UPR signalling networks under *U. parvum* infection. ER stress sensors such as PERK and IRE1 α were activated. miR-211 and miR-214 were induced by *U. parvum* infection in a PERK- and eIF2 α -dependent manner. Arrows indicate positive actions; circles indicate negative actions

are key molecules that inhibit the ER-stress cascade and result in an anti-apoptotic phenotype. PERK signalling induces miR-211, which in turn attenuates the stress-dependent expression of the proapoptotic transcription factor CHOP (Chitnis et al., 2012) and suppresses circadian regulators to promote cancer cell survival (Bu et al., 2018). miR-214 is known as a key molecule that controls cancer networks. The high miR-214 expression has been associated with unfavourable prognosis and poor response to therapy (Penna et al., 2015).

H. pylori VacA activates PERK and eIF2 α , which results in CHOP induction, in part mitochondrial dysfunction, and apoptosis (Akazawa et al., 2013; Chatre et al., 2017). We found that UpVF induced ER stress and mobilised two UPR signalling axes in HeLa cells, stemming from the activation of IRE1 and PERK. *U. parvum* was shown to cause the PERK-eIF2 α and IRE1 α signalling pathways, but unlike VacA, UpVF was found to inhibit both the downstream ATF4-CHOP signalling pathway and the signalling molecule XBP1 via miRNAs (Figures 1 and 3). The expression levels of miR-211, -214, -346 and -30-c-2*were increased in UpVF-expressing cells. Among these four miRs, the expression levels of miR-211 and -214 were significantly higher than those of miR-346 and -30-c-2*. We further focused on miR-211 and -214 (Figure 3c).

Multiple steps are needed to promote malignant cell transformation with a long latency. However, in the mouse embryonic cell line, C2H, infected with *M. fermentans*, a persistent infection (through 18 passages) resulted in an irreversible transformation. In contrast, all malignant changes were restored if mycoplasma was eradicated by ciprofloxacin treatment during passage 11 (Tsai et al., 1995). This classical observation begs the question of whether UpVF is essential for the continuity of the anti-apoptotic phenotype is established. We used a stable transformant of UpVF to examine this question. While screening for this stable transformant in HeLa and CaSki cells, host cells with large vacuoles were eradicated, suggesting that the high amount of UpVF expressed in the host cells was toxic. In contrast, a lower, limited expression of UpVF might allow host cell survival, resulting in the anti-apoptotic phenotype.

The association between oncogenic strains of human papillomavirus and cervical cancer is well established. Our experiments showed that UpVF might potentially worsen cancer-related outcomes. X-ray irradiation is known to induce DNA double-stranded breaks, the generation of ROS, G2/M-phase arrest, and cellular apoptosis (Zhao et al., 2019). Cisplatin is a cytotoxic drug that binds with DNA; it causes apoptosis by damaging the DNA (Ghosh, 2019). Paclitaxel initiates apoptosis through the checkpoint of mitotic spindle assembly, aberrant activation of cyclin-dependent kinases and c-Jun N-terminal kinase/stress-activated protein kinase are shown to be involved in paclitaxel-induced apoptosis (Wang, Wang, & Soong, 2000). We uncovered new aspects of UpVF associated with miRs expression that oppose ER stress-induced apoptosis. However, the mechanisms underlying UpVF resistance to X-rays and anticancer drugs are not fully understood. Human infection with Ureaplasma sp. has been estimated to be as high as 80% of adults (Waites, Xiao, Paralanov, Viscardi, & Glass, 2012); however, the significance of *Ureaplasma* sp. as a pathogen is still controversial (Viscardi, 2010). This study adds weight

to the idea that *U. parvum* infection may be associated with oncogenesis. We believe that elucidating the antitherapeutic mechanisms of ureaplasmas on cervical cancer resistance in detail will shed light on the utility of eradication of the chronic ureaplasma infection/colonisation in women.

4 | EXPERIMENTAL PROCEDURES

4.1 | Cells, bacteria and plasmids

U. parvum serovar 3 strain SV3F4 (Up-F4) was cultured and purified, as described previously (Wu et al., 2014). Bacterial open reading frames (ORFs) were amplified by PCR from genomic DNA prepared from purified *U. parvum* (Wu et al., 2014). *Saccharomyces cerevisiae* strain MTY483 was also used in this study (Tabuchi et al., 2009).

Expression clones were constructed by LR reaction with two types of destination vectors, pEF1/B2B1/V5-DEST and pEF/B2H1/SV-DEST, and two types of entry clones (Invitrogen Co. Carlsbad, CA) according to the manufacturer's instructions. pENTR-L1-sdk-EGFP-R3 and pENTR-L3-UpVF-*L2 were constructed by MultiSite Gateway® cloning of attB-PCR fragments amplified from cDNA plasmids of ER (Calreticulin, GenBank accession no. AY796115) and UpVF (GenBank accession no. AP014584, *UP3_c0403*). The construction of EGFP entry clones was described previously (Sone et al., 2008). The PCR primers used were as follows: ER (FW: 5'- GCTTCGAAGGAGAT AGAACCATGCTGCTGCCCGTCCCCCTG -3' RV: 5'- GTTG TCAC AGCTCATCCTTCTTGTACAGCTCGTC -3'), UpVF (FW: 5'- GGGGAC AACTTTGTATAATAAAGTTGATGATGAATGAATGATTTAATTTTAATACC -3').

4.2 | Cell culture and stable transformants

HeLa cells were incubated in Dulbecco's modified Eagle's minimum essential medium (DMEM; Thermo Fisher Scientific, MA) and RPMI 1640 (Thermo Fisher Scientific) supplemented with 10% fetal bovine serum (FBS; Sigma-Aldrich Co. LLC) at 37°C and 5% CO₂. The productions of stable transformants were described previously (Nishiumi et al., 2009). Transfection of HeLa and CaSki cells with the expression clones (EGFP-UpVF and EGFP) was performed using FuGENE® HD (Promega Corporation, Madison, WI) according to the manufacturer's instructions. Cotransfection with the expression clones, the pEXPR series described above and the φC31 integrase expression clone pJTI™ PhiC31 Int (Invitrogen™) was performed at a mass ratio of 1:1. After culturing in a 6-well plate for 24 hr, the approximate numbers of the transiently transformed cells were determined by fluorescence microscopy, and the cells were split among 10 cm plates and cultured. After 48 hr of transfection, the cells were selected in a medium containing 2-4 µg/mL blasticidin S HCl (Sigma-Aldrich). Selection continued for 14 days, after which the colonies became visible. Individual colonies were transferred using a pipette tip to individual wells of a 24-well plate. Surviving colonies were expanded for stock.

4.3 | Labelling U. parvum cell

In this study, we used the clinical isolates of *U. parvum* serovar 3 derived from human placenta of preterm delivery at 26 weeks of gestation (*U. parvum* OMC-P162). The *U. parvum* were cultured in 2 mL UMCHs medium (Namba et al., 2010) at 37°C overnight. The *U. parvum* label has been described previously (Nishiumi et al., 2017).

4.4 | *U. parvum* and JCVI-syn3B infection of culture cells

The HeLa cells and several stable transformant cells were grown on poly-L-lysine-coated glass coverslips (13 mm: Matsunami Glass Ind. Ltd., Osaka, Japan) to approximately 70% confluence. These cells were initially washed with PBS and then infected with *U. parvum* (1.5 \times 10 6 cfu) or JCVI-syn3B (2.7 \times 10 7 copies), and two JCVI-syn3B strains, Syn-MBA (0.9 \times 10 7 copies) and Syn-MBA-UpVF (1.0 \times 10 7 copies), for infection assays. Dil-labelled *U. parvum* or JCVI-syn3B, Syn-MBA, Syn-MBA-UpVF, suspended in 1 mL of DMEM with 2% FBS and used for infection. HeLa cells were infected with *U. parvum* for 0, 3, 6 or 24 hr, with JCVI-syn3B, Syn-MBA and Syn-MBA-UpVF for 6, 24, 48 and 72 hr at 37 $^\circ$ C under a 5% CO $_2$ atmosphere.

4.5 | ROS assay

HeLa cells were placed on poly-L-lysine-coated glass coverslips at a density of 4 \times 10⁴ cells/well, and the cells were incubated for 24 hr before further use. The cells were treated with 5 mM NAC (Sigma-Aldrich) for 1 hr before transfection. The HeLa cells were infected with Dil-labelled *U. parvum* or transient transfection with pEGFP-C1 and pEGFP-UpVF plasmid by incubation for 24 hr. The infected cells were washed with PBS. Next, the cells were incubated for an additional 30 min at 37°C and stained with 5 μ M CellROX reagent (Invitrogen). After incubation, the cells were washed three times with PBS. The cells were fixed 4% paraformaldehyde in PBS for 15 min at room temperature and subjected to immunostaining.

4.6 | Immunofluorescence and microscopy

After each period of infection, the *U. parvum* or Syn-MBA, Syn-MBA-UpVF suspension was gently removed, and each well with cell monolayer was washed three times with PBS. The infected HeLa cells were fixed with 4% paraformaldehyde in PBS for 15 min at room temperature, permeabilised with 0.1% Triton X-100 for 10 min, and blocked with 2% bovine serum albumin (BSA) for 1 hr at room temperature. The cells were incubated with primary antibodies, chicken polyclonal to calreticulin-ER Marker (ac14234, Abcam), MBA rabbit polyclonal antibody (1:500), affinity-purified rabbit polyclonal anti-UpVF (44–53) (1:200) antibody was raised against a synthetic peptide corresponding to the amino acid number from 44 to 53 of UpVF (Eurofins Genomics

KK) diluted with 2% BSA in PBS at 4°C overnight. Next, the cells were stained with species-specific Alexa Fluor 488 F(ab')2 fragment of goat anti-mouse antibody (Molecular Probes®), Alexa Fluor 568 goat anti-chicken IgG [H + L] antibody (Life Technologies), 4',6-diamidino-2-phenylindole (DAPI; Roche Diagnostic Co., Indianapolis, IN), PI (DO JINDO LABORATORIES, Japan) for 1 hr at room temperature. For immunofluorescence, a fluorescence microscope (Eclipse Ti; Nikon Co., Tokyo, Japan) with a filter set for CFP/GFP/TexRed (86,009; Chroma Technology Co., Bellow Falls, VT) was used.

4.7 | Electron microscopy

HeLa cells were cultured on a chamber slide at a density of 4×10^4 cells/slide and incubated for 24 hr before use. The cells were infected with $\it U.~parvum$ by incubation for 1–24 hr. The infected cells were fixed in 2.5% glutaraldehyde for 2 hr. Then, the $\it U.~parvum$ -infected cells were washed three times with phosphatase buffer (PB) and post-fixed in PB 1% osmium tetroxide for 30 min on ice. The fixed cells were dehydrated by dipping each of them through a series of ethanol solutions containing increasing ethanol concentrations and embedded in Epon resin (TAAB). Ultrathin sections were stained with lead citrate and uranyl acetate. The stained samples were subsequently observed under a Hitachi electron microscope (H-7650).

4.8 | Western blot analysis

The cells were harvested after *U. parvum* infection and lysed in lysis buffer containing 20 mM Tris-HCl (pH 7.5), 1% Nonidet P-40, 0.1 M NH₄SO₄, 10% glycerol and protease inhibitor cocktail set III (Calbiochem®, Merck KGaA, Darmstadt, Germany). Lysates were clarified by pipetting and rotated for 30 min at 4°C. Insoluble material was removed by centrifugation (15,000 \times g). Equal amounts of protein were loaded on a 5%-20% SDS-PAGE gradient gel and transferred to PVDF membranes (GE Healthcare Life Sciences, Buckinghamshire, UK). CHOP (L63F7) mouse monoclonal antibody (1:1000) (Cell Signalling), phosphoelF2a (Ser51) antibody (1:1000) (Cell Signalling), elF2 α antibody (1:1000) (Cell Signalling), BiP (C50B12) rabbit monoclonal antibody (1:1000) (Cell Signalling), IRE1α (14C10) rabbit mAb (1:1000) (Cell Signalling), ATF4 (D4B8) rabbit mAb (1:1000) (Cell Signalling), XBP1 (D2C1F) rabbit mAb (1:1000) (Cell Signalling), PARP (1:1000) (Cell Signalling), cleaved caspase 3 (Asp175) rabbit mAb (1:1000) (Cell Signalling) and MBA rabbit polyclonal antibody (1:1000) (Uchida et al., 2013) were used to detect protein expression patterns. Affinity-purified rabbit polyclonal anti-UpVF (14-27) (1:1000) antibody was raised against a synthetic peptide corresponding to the amino acid number from 14 to 27 of UpVF (Eurofins Genomics KK) for western blot analysis. After incubation with horseradish peroxidase-conjugated affinity-purified anti-mouse (Rockland Immunochemicals Inc., Gilbertsville, PA) or goat anti-rabbit (Rockland Immunochemicals) secondary antibodies, the blots were visualised using an enhanced chemiluminescence detection system (PerkinElmer Inc. Waltham, MA). The blots were also probed for glyceraldehyde-3-phosphate dehydrogenase (GAPDH), used as a loading control.

4.9 | Construction of *U. parvum-*array library

We constructed a library to express 32 ureaplasmal genes of unknown function in yeast cells, as described previously (Tabuchi et al., 2009). Individual bacterial ORFs were amplified by PCR using a specific pair of primers from genomic DNA prepared from purified *U. parvum* (-Table S4) (Wu et al., 2014). Oligonucleotides were designed such that the 3' end was specific to the gene of interest, and the 5' end partially overlapped the sequences of *attB*-adapter primers, as described in the Gateway technology instruction manual (Invitrogen). The *attB*-flanked PCR products were purified from agarose gel and cloned into pDONR221 vector by BP reaction to generate the *U. parvum*-entry clone array library. Subsequently, the inserts of the entry clones were cloned into pMT830 by LR reaction to generate the *U. parvum*-yeast expression array library. Partial sequences of *U. parvum*-DNA fragments cloned into pDONR221 were confirmed by an automated DNA sequencer (Applied Biosystems, Foster, CA).

4.10 | Pathogen protein screening in yeast by growth inhibitory phenotype

Previously we developed a functional high-throughput screening system for pathogen effectors in yeast (Tabuchi et al., 2009). This system is the pathogen effector screening system combining a Tet-Off promoter and Gateway-cloning technology system. Using this system, we performed to screen for the pathogen protein candidates from *U. parvum*.

The U. parvum-yeast expression array library, which contains ureaplasmal 32 ORFs, was transferred into a diploid yeast strain, MTY483, by a one-step transformation method as described previously (Tabuchi et al., 2009). The transformants were grown on SC-Ura/galactose square plates with 20 µg/mL of doxycycline at 30°C for 3 days. The colonies were picked using a 96-pin replicator and suspended in 100 µL PBS in 96-well microplates. The cell suspensions were further diluted 10- and 100-fold for SC-Ura/galactose. And then, 5 µL aliquots of diluted cell suspensions were spotted on SC-Ura / galactose plates with or without doxycycline. Plates were cultured at 30°C for 2-3 days. Relative growths were compared with yeast strains expressing EGFP alone or known pathogen effectors such as SopE2 and YpkA. The plasmids containing pathogen protein candidates obtained from the first screening were retransformed into MTY483, subsequently confirming the growth inhibition abilities by spotting in 10-fold serial dilution. The positive clones from the second screening were defined as the pathogen protein candidates.

4.11 | miRNA microarray analysis and Taqman assays

Total RNA was extracted from 1.5×10^5 HeLa cells using a ReliaPrep miRNA cell and Tissue Miniprep System (Promega Corporation, Madison, WI) and following the manufacture protocol. Total RNA was sent to Filgen® Corporation (Nagoya, Japan).

RT reaction was performed on 5 μ L total RNA, using the TaqMan MicroRNA Reverse Transcription Kit and a Custom TaqMan RT Primer Pool (Thermo Fisher Scientific), according to the manufacture's instruction. miRNA expression was analysed using TaqMan MicroRNA assays (Thermo Fisher Scientific): U6 (001973), hsa-miR-211 (00514), hsa-miR-30c-2* (002110), hsa-miR-708 (002341), hsa-miR-346 (000553) and hsa-miR-214 (002306).

4.12 | 3D digital PCR

We combined 1 μ L RT product with 5.75 μ L nuclease-free H₂O, 7.5 μ L QuantStudio[™] 3D Digital PCR Master Mix, 0.75 μ l TaqMan MicroRNA Assay (20×). This sample mix was added to each chip and loaded on a ProFlex[™] 2x Flat PCR System. Absolute quantification was determined using the QuantStudio 3D Digital PCR System (Thermo Fisher Scientific) and analysed with QuantStudio 3D AnalysisSuite Cloud software (Thermo Fisher Scientific).

4.13 | miRNA transfection

miRNA-negative control (NCSTUD002, Sigma-Aldrich), miR-211 inhibitor (MH10168) and miR-214 inhibitor (MH12921) were obtained from Ambion, Life Technologies. Transient transfections of 5 nM of miRNA inhibitors were achieved into stably expressing EGFP or EGFP-UpVF HeLa, or those of CaSki cells using Lipofectamine RNAiMAX (13,778,750, Life Technologies). Cells were incubated for 48 hr at 37°C then analysed by western blotting.

4.14 | TUNEL staining to determine cell apoptosis

Cells transfected with miR inhibitor for 24 hr were stained using a Click-iT Plus TUNEL Assay (for in situ apoptosis detection, Alexa Fluor 594 dye, Molecular Probes) according to the manufacturer's instructions. Ten visual fields in each sample were selected at random, and the average number of apoptotic cells per 150 cells was determined. The apoptotic index was calculated according to the following formula: apoptotic index (%) = (number of positive cells/total number of cells) \times 100.

4.15 | Cell counting Kit-8 assay

The cell viability was evaluated by Cell Counting Kit-8 (CCK8, Dojindo) assay. The cells were seeded into 96-well plates (5 \times 10 3 cells/well) and cultured overnight. Then, cells were treated with *U. parvum* (5 \times 10 4 CFU, 3 hr) or transient transfection of 0.1 µg/well of pEGFP-C1 (Addgene) or pEGFP-UP3_c0403 plasmid for 24 hr. Various indicated concentrations of actinomycin D (Sigma-Aldrich) for 6 hr, and cisplatin (Sigma-Aldrich), paclitaxel (FUJIFILM Wako Pure Chemical Co. Japan) for 24 hr. At the end of incubation, 10 µL CCK8 were

added onto cells. The cell viability was calculated as follows: cell viability (%) = [(OD of treated cells – OD of blank)/(OD of control cells – OD of blank)] \times 100. All assays were performed with at least three independent experiments.

4.16 | Radiation and colony formation assay

An X-ray generator system (MBR-1520 A-2, HITACHI, Tokyo, Japan) was used as the X-ray source. The HeLa and CaSki cells were treated with the dose at (HeLa; 2–8 Gy, CaSki; 0.5–2 Gy). The cells were further cultured in a complete medium for 14 days. Cells were plated in 6-well culture plates at a density of 200 cells/well. Three wells of cells were used for each group. After incubation for 14 days at 37°C, cells were washed twice with PBS and stained with 0.5% crystal violet. The number of colonies (>50 cells) was counted on an inverted microscope. The surviving fraction was calculated as follows: number of colonies/number of plated cells.

4.17 | Expression of MBA and UpVF in JCVI-svn3B

JCVI-syn3B cells were cultured in SP4 media at a pH of 6.3-6.8, as described elsewhere (Hutchison 3rd et al., 2016). U. parvum serovar 3 strain SV3F4 (Up-F4) was cultivated, and CDSs were amplified by PCR using purified genomic DNA of prepared U. parvum (Wu et al., 2014). The MBA gene was amplified from the SV3F4 genome by PCR using a specific primer pair SyMBA F1 and SyMBA R2 (-Table S2), while the promoter (spiralin gene from Spiroplasma citri: Pspi) was amplified from the pSD132 vector using the primer pair SyMBA F2 and SyUpVF R1. Nhel sites were introduced in the primers of mba and promoter regions for PCR amplification. The amplified products were then used for overlapping PCR (SyMBA F1, SyUpVF R1) assays. This product was inserted into the Nhel site of pSD128 vector. For the coexpression of MBA and UpVF, the Pspi and PxyltetO2 promoter regions were amplified from pSD079 vector with the primer pair MBA-UpVF Vector1 F1 and MBA-UpVF vector1 R2. The MBA and UpVF-encoding genes were amplified with the primer pair SyMBA F1 and MBA-UpVF vector R1, or SyUpVF F1 and SyUpVF R2. Nhel sites were designed in the primers used for PCR-amplifying MBA and UpVF. The amplified product of overlapping PCR (SyUpVF F1 and SyMBA F1) was inserted into the Nhel site of pSD128 vector (Figure S6). The JCVI-syn3B cells were transformed with the pSynpSyn-MBA-UpVF-expression plasmids et al., 2010). Individual colonies were selected and grown in SP4 medium, and their expression was confirmed by western blotting.

The quantification of JCVI-syn3B and its derivative bacteria was assessed by quantitative real-time PCR method by using the QuantiTect® SYBR® Green PCR Kit (QIAGEN) using the Chromo 4 Real-time PCR System (MJ Research). The PCR primers used were as follows: Syn3-16S F1; 5'-TAACATTAAGTTGAGAACTC-3' and Syn3-16S R1; 5'-GTTAAGCTACCTACTTCTGG-3'.

4.18 | Low vacuum scanning electron microscopy

HeLa cells were placed on a chamber slide at a density of 2×10^4 cells/slide and incubated 24 hr before use, and then infected with JCVI-syn3B, Syn-MBA or Syn-MBA-UpVF for the indicated periods. The post-infection cells were fixed with 2% glutaraldehyde and stored overnight, washed with PBS thrice, resuspended in PBS and dehydrated in an ascending ethanol series. The samples were covered for 30 min at room temperature with a platinum blue solution (TI-blue Staining Kit, Nisshin EM Co., Ltd., Tokyo, Japan), adjusted to pH 9.0. After washing with distilled water for 1–2 min, the SEM images were obtained using a low SEM microscope (Miniscope® TM3030 plus; Hitachi, Tokyo, Japan).

4.19 | Xenograft tumour growth

Immunodeficient KSN/Slc mice (6 weeks, female, 18-20 g body weight) were obtained from Japan SLC (Shizuoka, Japan). Xenografts were established by injection of 1×10^7 CaSki EGRP or EGFP-UpVF cells injected subcutaneously into the flank of each mouse. Animals were randomised, and treatments were initiated when tumour volume reached 100 mm³. Treatment was carried out with cisplatin intraperitoneally twice (7 mg/kg: weekly) or paclitaxel (FUJIFILM Wako Pure Chemical Co. Japan) (12 mg/kg) intraperitoneally every Monday, Wednesday and Friday, and then humanely killed once morbidity was evident. Tumour volume was measured three times per week. Tumour volume was defined as length \times width²/2. The tumour size limit at which mice were euthanised was based on major diameter (not more than 2 cm) or tumour volume reached at 2000 mm³. All mouse studies followed the fundamental ethical guidelines for the proper conduct of animal experiments and related activities in academic research institutions under the jurisdiction of the Ministry of Education, Culture, Sports, Science, and Technology of Japan and were approved by institutional committees at the Research Institute, Osaka Women's and Children's Hospital for animal and recombinant DNA experiments.

4.20 | Histological analysis

Tumours were fixed in 10% formalin, embedded with paraffin and sectioned. Haematoxylin and eosin staining and immunohistochemistry analysis were performed as described previously (Uchida et al., 2013). The following primary antibody used was anti-Ki-67 (Cell Signalling Technology).

4.21 | Statistical analysis

The statistical analyses were performed using the JMP® Pro software package (SAS Institute Inc., Cary, NC) and presented as means of experiments as indicated with usually three technical repeats within each experiment. Error bars represent mean ± standard error of the

mean (SEM). Student's t-test was used to examine the statistical significance of differences between the values of control and treatment groups, EGFP/EGFP-UpVF, Syn-MBA/Syn-MBA-UpVF. Differences were considered statistically significant at p < 0.05. Multiple comparisons between groups were analysed using one-way analysis of variance with a Tukey–Kramer post hoc test (Figures S1a,g, S3h and S6e). Kaplan–Meier analysis was used to measure survival analysis, and a comparison of overall survival between groups was performed using the log-rank test.

ACKNOWLEDGMENTS

We are grateful to Dr. Atsushi Miyawaki, (Riken, Japan) for KDEL construct, Dr. Samuel I. Miller (University of Washington) for Y. enterocolitica YpkA, Dr. Maria Molina (Universidad Complutense de Madrid, Spain) for S. typhimurium SopE2, Dr. Mitsuaki Tabuchi (Kagawa University, Japan) for MTY483, Yoshitaka Horiuchi (Kindai University, Japan) for supporting TEM analysis, Naoto Mizuno (WCH Osaka, Japan) for X-ray irradiation. This work was supported by research grants from the JSPS KAKENHI (JP26860859, JP17K10201 to FN; JP18K16788 to MY; JP17H04237, JP18K19191, JP19K07569, JP20H03564 to IY), AMED (JP20fk0108143 to IY), Grant Program for Biomedical Engineering Research from Nakatani Foundation for Advancement of Measuring Technologies in Biomedical Engineering, for Advanced of Measuring Technologies in Biomedical Engineering (IY), Japan, and by the United States National Science Foundation MCB program (1818344 and 1840320 to JIG).

CONFLICT OF INTEREST

No conflict of interest declared.

AUTHOR CONTRIBUTIONS

Conceptualization: Itaru Yanagihara. Data curation: Fumiko Nishiumi. Funding acquisition: Itaru Yanagihara, Fumiko Nishiumi, John I. Glass. Investigation: Fumiko Nishiumi, Yasuhiro Kawai, Yukiko Nakura, Michinobu Yoshimura, Heng-Ning Wu, Mitsuhide Hamaguchi. Visualisation: Fumiko Nishiumi, Itaru Yanagihara. Writing-review and editing: Shigeyuki Kakizawa, Yo Suzuki, John I. Glass. The authors declare no conflict of interest. All authors read and approved the manuscript.

DATA AVAILABILITY STATEMENT

The data that support the findings of this study are available from the corresponding author upon reasonable request.

ORCID

Mitsuhide Hamaguchi https://orcid.org/0000-0003-1146-898X Itaru Yanagihara https://orcid.org/0000-0001-9882-8196

REFERENCES

Akazawa, Y., Isomoto, H., Matsushima, K., Kanda, T., Minami, H., Yamaghchi, N., ... Nakao, K. (2013). Endoplasmic reticulum stress contributes to *helicobacter pylori* VacA-induced apoptosis. *PLoS ONE*, 8(12), e82322. https://doi.org/10.1371/journal.pone.0082322

- Avril, T., Vauleon, E., & Chevet, E. (2017). Endoplasmic reticulum stress signaling and chemotherapy resistance in solid cancers. *Oncogene*, 6(8), e373. https://doi.org/10.1038/oncsis.2017.72
- Bischof, L. J., Kao, C. Y., Los, F. C., Gonzalez, M. R., Shen, Z., Briggs, S. P., ... Aroian, R. V. (2008). Activation of the unfolded protein response is required for defenses against bacterial pore-forming toxin in vivo. *PLoS Pathogens*, 4(10), e1000176. https://doi.org/10.1371/journal.ppat. 1000176
- Bu, Y., Yoshida, A., Chitnis, N., Altman, B. J., Tameire, F., Oran, A., ... Diehl, J. A. (2018). A PERK-miR-211 axis suppresses circadian regulators and protein synthesis to promote cancer cell survival. *Nature Cell Biology*, 20(1), 104–115. https://doi.org/10.1038/s41556-017-0006-v
- Cao, S. S., & Kaufman, R. J. (2014). Endoplasmic reticulum stress and oxidative stress in cell fate decision and human disease. Antioxidants & Redox Signaling, 21(3), 396–413. https://doi.org/10.1089/ars.2014. 5851
- Chandrahas, V. K., Han, J., & Kaufman, R. J. (2018). Coordinating organismal metabolism during protein Misfolding in the ER through the unfolded protein response. Current Topics in Microbiology and Immunology, 414, 103–130. https://doi.org/10.1007/82_2017_41
- Chatre, L., Fernandes, J., Michel, V., Fiette, L., Ave, P., Arena, G., ... Touati, E. (2017). Helicobacter pylori targets mitochondrial import and components of mitochondrial DNA replication machinery through an alternative VacA-dependent and a VacA-independent mechanisms. Scientific Reports, 7(1), 15901. https://doi.org/10.1038/s41598-017-15567-3
- Chauhan, S., Kumar, S., Jain, A., Ponpuak, M., Mudd, M. H., Kimura, T., ... Deretic, V. (2016). TRIMs and galectins globally cooperate and TRIM16 and Galectin-3 co-direct autophagy in endomembrane damage homeostasis. *Developmental Cell*, 39(1), 13–27. https://doi.org/10. 1016/j.devcel.2016.08.003
- Chitnis, N. S., Pytel, D., Bobrovnikova-Marjon, E., Pant, D., Zheng, H., Maas, N. L., ... Diehl, J. A. (2012). miR-211 is a prosurvival microRNA that regulates chop expression in a PERK-dependent manner. *Molecular Cell*, 48(3), 353–364. https://doi.org/10.1016/j.molcel.2012. 08.025
- Chu, Q., Martinez, T. F., Novak, S. W., Donaldson, C. J., Tan, D., Vaughan, J. M., ... Saghatelian, A. (2019). Regulation of the ER stress response by a mitochondrial microprotein. *Nature Communications*, 10(1), 4883. https://doi.org/10.1038/s41467-019-12816-z
- Curtin, J. F., Donovan, M., & Cotter, T. G. (2002). Regulation and measurement of oxidative stress in apoptosis. *Journal of Immunological Methods*, 265(1-2), 49-72. https://doi.org/10.1016/s0022-1759(02) 00070-4
- Delmotte, P., & Sieck, G. C. (2019). Endoplasmic reticulum stress and mitochondrial function in airway smooth muscle. Frontiers in Cell and Development Biology, 7, 374. https://doi.org/10.3389/fcell.2019.00374
- Drago, F., Herzum, A., Ciccarese, G., Dezzana, M., Casazza, S., Pastorino, A., ... Parodi, A. (2016). *Ureaplasma parvum* as a possible enhancer agent of HPV-induced cervical intraepithelial neoplasia: Preliminary results. *Journal of Medical Virology*, 88(12), 2023–2024. https://doi.org/10.1002/jmv.24583
- Dybvig, K., & Voelker, L. L. (1996). Molecular biology of mycoplasmas. Annual Review of Microbiology, 50, 25–57. https://doi.org/10.1146/annurev.micro.50.1.25
- Ghosh, S. (2019). Cisplatin: The first metal based anticancer drug, 88.
- Gibson, D. G., Glass, J. I., Lartigue, C., Noskov, V. N., Chuang, R. Y., Algire, M. A., ... Venter, J. C. (2010). Creation of a bacterial cell controlled by a chemically synthesized genome. *Science*, 329(5987), 52–56. https://doi.org/10.1126/science.1190719
- Hossain, T., Deter, H. S., Peters, E. J., & Butzin, N. C. (2021). Antibiotic tolerance, persistence, and resistance of the evolved minimal cell. Mycoplasma mycoides JCVI-Syn3B. bioRxiv, 24(5), 130641. https://doi.org/10.1101/2020.06.02.130641

- Hutchison, C. A., 3rd, Chuang, R. Y., Noskov, V. N., Assad-Garcia, N., Deerinck, T. J., Ellisman, M. H., ... Venter, J. C. (2016). Design and synthesis of a minimal bacterial genome. *Science*, 351(6280), aad6253. https://doi.org/10.1126/science.aad6253
- Ito, K., Akai, K., Nishiumi, F., Nakura, Y., Wu, H. N., Kurata, T., ... Yanagihara, I. (2021). Ability of *Ureaplasma parvum* to invade mouse sperm, fertilize eggs through infected sperm, and impair mouse sperm function and embryo development. F&S Science, 2(1), 13–23. https:// doi.org/10.1016/j.xfss.2020.12.003
- Kornspan, J. D., & Rottem, S. (2012). The phospholipid profile of mycoplasmas. *Journal of Lipids*, 2012, 640762. https://doi.org/10.1155/2012/640762
- Lee, J., & Song, C. H. (2021). Effect of reactive oxygen species on the endoplasmic reticulum and mitochondria during intracellular pathogen infection of mammalian cells. *Antioxidants (Basel)*, 10(6), 1–21. https://doi.org/10.3390/antiox10060872
- Lesser, C. F., & Miller, S. I. (2001). Expression of microbial virulence proteins in *Saccharomyces cerevisiae* models mammalian infection. *The EMBO Journal*, 20(8), 1840–1849. https://doi.org/10.1093/emboj/20.8.1840
- Loose, M., Hudel, M., Zimmer, K. P., Garcia, E., Hammerschmidt, S., Lucas, R., ... Pillich, H. (2015). Pneumococcal hydrogen peroxide-induced stress signaling regulates inflammatory genes. *The Journal of Infectious Diseases*, 211(2), 306–316. https://doi.org/10.1093/infdis/jiu428
- Ma, Y., & Hendershot, L. M. (2004). ER chaperone functions during normal and stress conditions. *Journal of Chemical Neuroanatomy*, 28(1–2), 51– 65. https://doi.org/10.1016/j.jchemneu.2003.08.007
- Madden, E., Logue, S. E., Healy, S. J., Manie, S., & Samali, A. (2019). The role of the unfolded protein response in cancer progression: From oncogenesis to chemoresistance. *Biology of the Cell*, 111(1), 1–17. https://doi.org/10.1111/boc.201800050
- Mager, D. L. (2006). Bacteria and cancer: Cause, coincidence or cure? A review. Journal of Translational Medicine, 4, 14. https://doi.org/10. 1186/1479-5876-4-14
- Maman, S., & Witz, I. P. (2018). A history of exploring cancer in context. Nature Reviews Cancer, 18(6), 359–376. https://doi.org/10.1038/ s41568-018-0006-7
- McQuiston, A., & Diehl, J. A. (2017). Recent insights into PERK-dependent signaling from the stressed endoplasmic reticulum. F1000Research, 6, 1897. https://doi.org/10.12688/f1000research.12138.1
- Miyake, M., Ohnishi, K., Hori, S., Nakano, A., Nakano, R., Yano, H., ... Fujimoto, K. (2019). Mycoplasma genitalium infection and chronic inflammation in human prostate Cancer: Detection using prostatectomy and needle biopsy specimens. Cell, 8(3), 1–11. https://doi.org/ 10.3390/cells8030212
- Monecke, S., Helbig, J. H., & Jacobs, E. (2003). Phase variation of the multiple banded protein in Ureaplasma urealyticum and *Ureaplasma parvum*. *International Journal of Medical Microbiology*, 293(2–3), 203–211. https://doi.org/10.1078/1438-4221-00239
- Namba, F., Hasegawa, T., Nakayama, M., Hamanaka, T., Yamashita, T., Nakahira, K., ... Yanagihara, I. (2010). Placental features of chorioamnionitis colonized with Ureaplasma species in preterm delivery. *Pediatric Research*, 67(2), 166–172. https://doi.org/10.1203/PDR. 0b013e3181c6e58e
- Namiki, K., Goodison, S., Porvasnik, S., Allan, R. W., Iczkowski, K. A., Urbanek, C., ... Rosser, C. J. (2009). Persistent exposure to Mycoplasma induces malignant transformation of human prostate cells. *PLoS ONE*, 4(9), e6872. https://doi.org/10.1371/journal.pone.0006872
- Newlaczyl, A. U., & Yu, L. G. (2011). Galectin-3-a jack-of-all-trades in cancer. Cancer Letters, 313(2), 123–128. https://doi.org/10.1016/j.canlet. 2011.09.003
- Ning, J. Y., & Shou, C. C. (2004). Mycoplasma infection and cancer. *Ai Zheng*, 23(5), 602–604.
- Nishiumi, F., Ogawa, M., Nakura, Y., Hamada, Y., Nakayama, M., Mitobe, J., ... Yanagihara, I. (2017). Intracellular fate of *Ureaplasma parvum*

- entrapped by host cellular autophagy. *Microbiology*, *6*(3), e00441. https://doi.org/10.1002/mbo3.441
- Nishiumi, F., Sone, T., Kishine, H., Thyagarajan, B., Kogure, T., Miyawaki, A., ... Imamoto, F. (2009). Simultaneous single cell stable expression of 2-4 cDNAs in HeLaS3 using psiC31 integrase system. Cell Structure and Function, 34(1), 47–59. https://doi.org/10.1247/csf. 08044
- Olarerin-George, A. O., & Hogenesch, J. B. (2015). Assessing the prevalence of mycoplasma contamination in cell culture via a survey of NCBI's RNA-seq archive. *Nucleic Acids Research*, 43(5), 2535–2542. https://doi.org/10.1093/nar/gkv136
- Paiva, C. N., & Bozza, M. T. (2014). Are reactive oxygen species always detrimental to pathogens? Antioxidants & Redox Signaling, 20(6), 1000– 1037. https://doi.org/10.1089/ars.2013.5447
- Papaioannou, A., & Chevet, E. (2018). Driving Cancer tumorigenesis and metastasis through UPR signaling. Current Topics in Microbiology and Immunology, 414, 159–192. https://doi.org/10.1007/82_2017_36
- Pardini, B., De Maria, D., Francavilla, A., Di Gaetano, C., Ronco, G., & Naccarati, A. (2018). MicroRNAs as markers of progression in cervical cancer: A systematic review. *BMC Cancer*, 18(1), 696. https://doi.org/10.1186/s12885-018-4590-4
- Payne, M. S., Ireland, D. J., Watts, R., Nathan, E. A., Furfaro, L. L., Kemp, M. W., ... Newnham, J. P. (2016). *Ureaplasma parvum* genotype, combined vaginal colonisation with Candida albicans, and spontaneous preterm birth in an Australian cohort of pregnant women. *BMC Pregnancy and Childbirth*, 16(1), 312. https://doi.org/10.1186/s12884-016-1110-x
- Pelletier, J. F., Sun, L., Wise, K. S., Assad-Garcia, N., Karas, B. J., Deerinck, T. J., ... Strychalski, E. A. (2020). Genetic requirements for cell division in a genomically minimal cell. *Cell* bioRxiv, 184(9), 2430– 2440. https://doi.org/10.1101/2020.10.07.326892
- Peng, R. Q., Wan, H. Y., Li, H. F., Liu, M., Li, X., & Tang, H. (2012). Micro-RNA-214 suppresses growth and invasiveness of cervical cancer cells by targeting UDP-N-acetyl-alpha-D-galactosamine:Polypeptide N-acetylgalactosaminyltransferase 7. The Journal of Biological Chemistry, 287(17), 14301–14309. https://doi.org/10.1074/jbc.M111. 337642
- Penna, E., Orso, F., & Taverna, D. (2015). miR-214 as a key hub that controls cancer networks: Small player, multiple functions. *The Journal of Investigative Dermatology*, 135(4), 960–969. https://doi.org/10.1038/jid.2014.479
- Pillich, H., Loose, M., Zimmer, K. P., & Chakraborty, T. (2016). Diverse roles of endoplasmic reticulum stress sensors in bacterial infection. *Molecular Cell Pediatrics*, 3(1), 9. https://doi.org/10.1186/s40348-016-0037-7
- Qu, X., Gao, D., Ren, Q., Jiang, X., Bai, J., & Sheng, L. (2018). miR-211 inhibits proliferation, invasion and migration of cervical cancer via targeting SPARC. Oncology Letters, 16(1), 853–860. https://doi.org/10.3892/ol.2018.8735
- Rittenschober-Bohm, J., Waldhoer, T., Schulz, S. M., Pimpel, B., Goeral, K., Kasper, D. C., ... Berger, A. (2019). Vaginal *Ureaplasma parvum* serovars and spontaneous preterm birth. *American Journal of Obstetrics and Gynecology*, 220(6), 594.e591–594.e599. https://doi.org/10.1016/j. ajog.2019.01.237
- Rodriguez-Escudero, I., Rotger, R., Cid, V. J., & Molina, M. (2006). Inhibition of Cdc42-dependent signalling in Saccharomyces cerevisiae by phosphatase-dead SigD/SopB from Salmonella typhimurium. Microbiology (Reading), 152(Pt 11), 3437–3452. https://doi.org/10.1099/mic.0. 29186-0
- Rodriguez-Pachon, J. M., Martin, H., North, G., Rotger, R., Nombela, C., & Molina, M. (2002). A novel connection between the yeast Cdc42 GTPase and the Slt2-mediated cell integrity pathway identified through the effect of secreted Salmonella GTPase modulators. *The Journal of Biological Chemistry*, 277(30), 27094–27102. https://doi.org/10.1074/jbc.M201527200

- Rogers, M. B. (2011). Mycoplasma and cancer: In search of the link. Oncotarget, 2(4), 271–273. https://doi.org/10.18632/oncotarget.264
- Sharma, T., Hamilton, R., & Mandal, C. C. (2015). miR-214: A potential biomarker and therapeutic for different cancers. *Future Oncology*, 11(2), 349–363. https://doi.org/10.2217/fon.14.193
- Sone, T., Yahata, K., Sasaki, Y., Hotta, J., Kishine, H., Chesnut, J. D., & Imamoto, F. (2008). Multi-gene gateway clone design for expression of multiple heterologous genes in living cells: Modular construction of multiple cDNA expression elements using recombinant cloning. *Journal of Biotechnology*, 136(3-4), 113-121. https://doi.org/10.1016/j.jbiotec.2008.06.006
- Tabuchi, M., Kawai, Y., Nishie-Fujita, M., Akada, R., Izumi, T., Yanatori, I., ... Kishi, F. (2009). Development of a novel functional high-throughput screening system for pathogen effectors in the yeast *Saccharomyces* cerevisiae. Bioscience, Biotechnology, and Biochemistry, 73(10), 2261– 2267. https://doi.org/10.1271/bbb.90360
- Tantengco, O. A. G., & Yanagihara, I. (2019). Current understanding and treatment of intra-amniotic infection with Ureaplasma spp. *The Journal* of Obstetrics and Gynaecology Research, 45(9), 1796–1808. https://doi. org/10.1111/jog.14052
- To, E. E., O'Leary, J. J., O'Neill, L. A. J., Vlahos, R., Bozinovski, S., Porter, C. J. H., ... Selemidis, S. (2020). Spatial properties of reactive oxygen species govern pathogen-specific immune system responses. Antioxidants & Redox Signaling, Brooks. R.D. 32(13), 982–992. https://doi.org/10.1089/ars.2020.8027
- Tsai, S., Wear, D. J., Shih, J. W., & Lo, S. C. (1995). Mycoplasmas and oncogenesis: Persistent infection and multistage malignant transformation. Proceedings of the National Academy of Sciences of the United States of America, 92(22), 10197–10201. https://doi.org/10.1073/pnas.92.22. 10197
- Uchida, K., Nakahira, K., Mimura, K., Shimizu, T., De Seta, F., Wakimoto, T., ... Yanagihara, I. (2013). Effects of *Ureaplasma parvum* lipoprotein multiple-banded antigen on pregnancy outcome in mice. *Journal of Reproductive Immunology*, 100(2), 118–127. https://doi.org/10.1016/j. iri.2013.10.001
- Urra, H., Dufey, E., Avril, T., Chevet, E., & Hetz, C. (2016). Endoplasmic reticulum stress and the hallmarks of Cancer. *Trends Cancer*, 2(5), 252– 262. https://doi.org/10.1016/j.trecan.2016.03.007
- Vande Voorde, J., Sabuncuoglu, S., Noppen, S., Hofer, A., Ranjbarian, F., Fieuws, S., ... Liekens, S. (2014). Nucleoside-catabolizing enzymes in mycoplasma-infected tumor cell cultures compromise the cytostatic activity of the anticancer drug gemcitabine. *The Journal of Biological Chemistry*, 289(19), 13054–13065. https://doi.org/10.1074/jbc. M114.558924
- Viscardi, R. M. (2010). Ureaplasma species: Role in diseases of prematurity. Clinics in Perinatology, 37(2), 393–409. https://doi.org/10.1016/j.clp. 2009.12.003
- Waites, K. B., Xiao, L., Paralanov, V., Viscardi, R. M., & Glass, J. I. (2012). Molecular methods for the detection of Mycoplasma and ureaplasma infections in humans: A paper from the 2011 William Beaumont Hospital symposium on molecular pathology. *The Journal of Molecular Diag*nostics, 14(5), 437–450. https://doi.org/10.1016/j.jmoldx.2012. 06.001
- Wakimoto, T., Uchida, K., Mimura, K., Kanagawa, T., Mehandjiev, T. R., Aoshima, H., ... Yanagihara, I. (2015). Hydroxylated fullerene: A potential antiinflammatory and antioxidant agent for preventing mouse preterm birth. American Journal of Obstetrics and Gynecology, 213(5), 708 e701-708 e709. https://doi.org/10.1016/j.ajog.2015. 07.017
- Wang, T. H., Wang, H. S., & Soong, Y. K. (2000). Paclitaxel-induced cell death: Where the cell cycle and apoptosis come together. *Cancer*, 88(11), 2619–2628. https://doi.org/10.1002/1097-0142(20000601) 88:11<2619::aid-cncr26>3.0.co;2-j
- Weng, I. C., Chen, H. L., Lo, T. H., Lin, W. H., Chen, H. Y., Hsu, D. K., & Liu, F. T. (2018). Cytosolic galectin-3 and -8 regulate antibacterial

- autophagy through differential recognition of host glycans on damaged phagosomes. *Glycobiology*, 28(6), 392–405. https://doi.org/10.1093/glycob/cwy017
- White, M. K., Pagano, J. S., & Khalili, K. (2014). Viruses and human cancers: A long road of discovery of molecular paradigms. *Clinical Microbiology Reviews*, 27(3), 463-481. https://doi.org/10.1128/CMR. 00124-13
- Wu, H. N., Nakura, Y., Motooka, D., Nakamura, S., Nishiumi, F., Ishino, S., ... Yanagihara, I. (2014). Complete genome sequence of *Ureaplasma parvum* Serovar 3 strain SV3F4, isolated in Japan. *Genome Announcements*, 2(3), e00256. https://doi.org/10.1128/genomeA.00256-14
- Xiaolei, C., Taot, H., Zongli, S., & Hongying, Y. (2014). The role of ureaplasma urealyticum infection in cervical intraepithelial neoplasia and cervical cancer. European Journal of Gynaecological Oncology, 35(5), 571–575.
- Ye, H., Song, T., Zeng, X., Li, L., Hou, M., & Xi, M. (2018). Association between genital mycoplasmas infection and human papillomavirus infection, abnormal cervical cytopathology, and cervical cancer: A systematic review and meta-analysis. Archives of Gynecology and Obstetrics, 297(6), 1377–1387. https://doi.org/10.1007/s00404-018-4733-5
- Zarei, O., Rezania, S., & Mousavi, A. (2013). Mycoplasma genitalium and cancer: A brief review. *Asian Pacific Journal of Cancer Prevention*, 14(6), 3425–3428. https://doi.org/10.7314/apjcp.2013.14.6.3425
- Zella, D., Curreli, S., Benedetti, F., Krishnan, S., Cocchi, F., Latinovic, O. S., ... Gallo, R. C. (2018). Mycoplasma promotes malignant transformation

- in vivo, and its DnaK, a bacterial chaperone protein, has broad oncogenic properties. *Proceedings of the National Academy of Sciences of the United States of America*, 115(51), E12005–E12014. https://doi.org/10.1073/pnas.1815660115
- Zhao, H., Zhuang, Y., Li, R., Liu, Y., Mei, Z., He, Z., ... Zhou, Y. (2019). Effects of different doses of X-ray irradiation on cell apoptosis, cell cycle, DNA damage repair and glycolysis in HeLa cells. *Oncology Letters*, 17(1), 42–54. https://doi.org/10.3892/ol.2018.9566

SUPPORTING INFORMATION

Additional supporting information may be found in the online version of the article at the publisher's website.

How to cite this article: Nishiumi, F., Kawai, Y., Nakura, Y., Yoshimura, M., Wu, H. N., Hamaguchi, M., Kakizawa, S., Suzuki, Y., Glass, J. I., & Yanagihara, I. (2021). Blockade of endoplasmic reticulum stress-induced cell death by *Ureaplasma parvum* vacuolating factor. *Cellular Microbiology*, e13392. https://doi.org/10.1111/cmi.13392